surface of the drying product became dry and rigid long before the center had dried out; the center dried and shrank much later than the outer surface did and pulled away from the rigid surface layers and caused a non-uniform shrinkage. Drying carrot in LPSSD, however, led to a more uniform shrinkage; in this case shrinkage seemed to occur because the carrot structure could not support its own weight and hence collapsed under gravitational force in the absence of moisture (Achanta and Okos, 2000). This is because LPSSD offered a milder drying condition (since the drying chamber was moister than in the case of vacuum drying). Dense or rigid large formation might not as much be formed in the case of LPSSD as in the case of vacuum drying. The photographs of carrot cubes both after drying and after rehydration are shown in Figure 6

Regarding the rehydration ability of carrot undergoing both drying processes it can be seen in Table 2 that carrot that underwent LPSSD had much better rehydration capability than that vacuum dried. This is also due to the formation of dense layers in the case of vacuum drying, which led to non-uniform shrinkage mentioned earlier; the rather dense and rigid layers prevented the re-adsorption of water and hence led to lower degrees of rehydration. This can also be seen from SEM photographs of Figures 7a and 7b, which show the microstructure of LPSSD and vacuum dried carrot, respectively. It is seen from these figures that carrot that underwent vacuum drying developed a rather dense layer and its pore distribution was rather non-uniform comparing with carrot that underwent LPSSD (see Figures 8a and 8b), which also did not have dense layer that prevented re-adsorption of water. It was also found that, in general, there existed an adverse relationship between the degree of rehydration and that of shrinkage.

Color Parameters

The changes of color parameters (Δa and ΔL) of carrot undergoing LPSSD and vacuum drying are listed in Table 3. It was observed that all dried carrot was redder than fresh carrot as can be seen from the positive Δa values. This is probably due to the concentration of color pigments in

carrot when moisture is removed. On the other hand, it was observed that almost all drying conditions (for both LPSSD and vacuum drying) yielded dried carrot with negative ΔL values, which implied that the dried carrot was slightly darker than the fresh one.

It can be observed from Table 3 that, when comparing the effects of different drying methods that LPSSD yielded carrot of redder and lighter colors than those obtained by vacuum drying. These results were similar to those reported by Caixeta et al. (2002) who compared the color values of potato chips undergoing impingement superheated steam drying and hot air drying. It was also found that lower drying temperatures gave redder and lighter dried carrot. This may be due to the fact that red color is attributed to the presence of β carotenes (Lin et al., 1998) and the degradation of β carotene in carrot is inversely proportional to the drying temperature (Pan et al., 1999). Operating pressure seems to have only a small effect on the colors of the dried carrot, however.

CONCLUSIONS

Detailed experimental evaluation of low-pressure superheated steam drying showed that, despite lower drying rates due to poorer convective heat transfer under reduced pressures, the process gave superior quality dried product compared to that obtained using conventional vacuum drying. It was observed that the effect of operating pressure was less significant than that of steam temperature. It is interesting to note that the operating pressure and temperature affected the shapes of the drying rate and temperature curves differently in steam drying and vacuum drying. The two drying techniques yielded differing structural and optical properties of the dried product. Steam drying provided better rehydration and a redder dried carrot than that obtained in vacuum drying over the operating parameter ranges studied.

ACKNOWLEDGEMENTS

The authors would like to express their sincere appreciation to the Thailand Research Fund (TRF) and the International Foundation for Science (Sweden) for supporting this study financially.

NOMENCLATURE

 m_P = mass of an empty pycnometer, g

 m_{Ph} = mass of a pycnometer filled with n-heptane, g

 m_{Phs} = mass of a pycnometer with sample and n-heptane, g

 m_s = masses of the sample, g

R = rehydration ratio, -

 $V = \text{volume, cm}^3$

 V_i = volume of fresh carrot, cm³

Greek letters

 ρ_{app} = apparent density, g/cm³

 ρ_h = density of n-heptane, g/cm³

REFERENCES

- Achanta, S.; Okos, M.R. Quality Changes during Drying of Food Polymers. In *Drying Technology* in *Agriculture and Food Science*, A.S. Mujumdar, Ed.; Science Publishers, Inc.: Enfield, 2000; 133-147.
- Caixeta, A.T.; Moraira, R.; Castell-Perez, M.E. Impingement Drying of Potato Chips. Journal of Food Process Engineering **2002**, 25(1), 63-90.
- Chen, S.R.; Chen, J.Y.; Mujumdar, A.S. Preliminary Study of Steam Drying of Silkworm Cocoons. Drying Technology **1992**, 10(1), 251-260.

- Cui, W.K.; Mujumdar, A.S. Paper Drying An Overview of Developments. In *Drying of Solids*, A.S. Mujumdar, Ed.; Wiley Eastern, New Delhi, 1986; 142-156.
- Douglas, W.J.M. Drying Paper in Superheated Steam. Drying Technology **1994**, 12(6), 1341-1355.
- Elustondo, D.; Elustondo, M.P.; Urbicain, M.J. Mathematical Modeling of Moisture Evaporation from Foodstuffs Exposed to Subatmospheric Pressure Superheated Steam. Journal of Food Engineering **2001**, 49(1), 15-24.
- Elustondo, D.M.; Mujumdar, A.S.; Urbicain, M.J. Optimum Operating Conditions in Drying Foodstuffs with Superheated Steam. Drying Technology **2002**, 20(2), 381-402.
- Iyota, H.; Nishimura, N.; Yoshida, M.; Nomura, T. Simulation of Superheated Steam Drying Considering Initial Steam Condensation. Drying Technology **2001**, 19(7), 1425-1440.
- Krokida, M.K.; Maroulis, Z. Quality Changes during Drying of Food Materials. In *Drying Technology in Agriculture and Food Science*, A.S. Mujumdar, Ed.; Science Publishers, Inc.: Enfield, 2000; 61-106.
- Krokida, M.K.; Oreopoulou, V.; Maroulis, Z.B. Modeling Shrinkage and Porosity during Vacuum Dehydration. International Journal of Food Science and Technology **1997**, 32(6) 445-458.
- Kumar, P.; Mujumdar, A.S. Superheated-Steam Drying: A Bibliography. Drying Technology **1990**, 8(1), 195-205.
- Lin, T.M.; Durance, T.D.; Scaman, C.H. Characterization of Vacuum Microwave, Air and Freeze Dried Carrot Slices. Food Research International **1998**, 31(2), 111-117.
- Moreira, R.G. Impingement Drying of Foods Using Hot Air and Superheated Steam. Journal of Food Engineering **2001**, 49(4), 291-295.
- Mujumdar, A.S. Recent Developments in Drying. *Annual Conference of the Indian Institute of Chemical Engineering*, Madras, India, 1981.

- Mujumdar, A.S. Superheated Steam Drying. In *Handbook of Industrial Drying*, A.S. Mujumdar, Ed.; Marcel Dekker: New York, 1995; 1071-1086.
- Mujumdar, A.S. Superheated Steam Drying Technology of the Future. In *Mujumdar's Practical Guide to Industrial Drying*, S. Devahastin, Ed.; Exergex: Brossard, Canada, 2000; 115-138.
- Pan, Y.K.; Zhao, L.J.; Dong, Z.X.; Mujumdar, A.S.; Kudra, T. Intermittent Drying of Carrot in a Vibrated Fluid Bed: Effect on Product Quality. Drying Technology **1999**, 17(10), 2323-2340.
- Pang, S.; Dakin, M. Drying Rate and Temperature Profile for Superheated Steam Vacuum Drying and Moist Air Drying of Softwood Lumber. Drying Technology **1999**, 17(6), 1135-1147.
- Potter, N.N.; Hotchkiss, J.H. Food science, 5th Ed.; An Aspen Publication: Gaithersburg, 1998.
- Potter, O.E; Beeby, C. Modelling Tube to Bed Heat Transfer in Fluidized Bed Steam Drying. In *Drying'86 Vol. 2*, A.S. Mujumdar, Ed.; Hemisphere: Washington, 1986; 595-603.
- Ratti, C. Shrinkage during Drying of Foodstuffs. Journal of Food Engineering 1994, 23(1), 91-95.
- Salin, J.G. Steam Drying of Wood Particles for Particleboard. In *Drying'86 Vol. 2*, A.S. Mujumdar, Ed.; Hemisphere: Washington, 1986; 572-574.
- Senda, Y.; Bando, Y.; Yasuda, K.; Nakamura, M.; Sugimura, Y.; Shibata, M. Development of Superheated Steam Dryer at Reduced Pressure. In *Proceeding of the 1st Asia -Pacific Drying Conference*, Bali, Indonesia, 2001; 247-256.
- Seyed-Yagoobi, J.; Li, Y.B.; Moreira, R.G.; Yamsaengsung, R. Superheated Steam Impingement Drying of Tortilla Chips. Drying Technology **1999**, 17(1&2), 191-213.
- Shibata, H.; Mada, J.; Funatsu, K. Prediction of Drying Curves on Sintered Spheres of Glass Beads in Superheated Steam under Vacuum. Industrial & Engineering Chemistry Research **1990**, 29(4), 614-617.
- Shibata, H.; Mada, J.; Shinohara, H. Drying Mechanism of Sintered Spheres of Glass Beads in Superheated Steam. Industrial & Engineering Chemistry Research 1988, 27(12), 2353-2362.
- Tang, Z.; Cenkowski, S.; Muir, W.E. Dehydration of Sugar-beet Pulp in Superheated Steam and Hot Air. Transactions of the ASAE **2000**, 43(3), 685-689.

Urbaniec, K.; Malczewski, J. Experimental Investigations of Beet Pulp Drying in Superheated Steam under Pressure. Drying Technology **1997**, 15(6-8), 2005-2011.

List of Tables

- Table 1. Average drying times of LPSSD and vacuum drying of carrot at various operating conditions
- Table 2. Physical properties of carrot undergoing LPSSD and vacuum drying at different drying conditions
- Table 3. Average values of Δa and ΔL of carrot undergoing LPSSD and vacuum drying at different operating conditions

Table 1. Average drying times of LPSSD and vacuum drying of carrot at various operating conditions.

Drying time of LPSSD (min)							
Pressure	Temperature (°C)						
(kPa)	60	70	80				
7	389	280	198				
10	N/A	290	210				
13	N/A	317	230				
Drying time of vacuum drying (min)							
Pressure	Temperature (°C)						
(kPa)	60	70	80				
7	235	205	159				
10	241	223	175				
13	255	265	206				

N/A implies that, at this condition, the final carrot moisture content of 0.07 kg/kg (d.b.) was not achievable

Table 2. Physical properties of carrot undergoing LPSSD and vacuum drying at different drying conditions.

Drying	Temperature	Pressure	Volume	Density	Shrinkage	Rehydration
Process	(°C)	(kPa)	(cm^3)	(g/cm^3)	(%)	ratio
LPSSD	T = 60°C	7	0.092 ± 0.002^{d}	1.43 ± 0.03^{a}	90.80 ± 0.09^{ab}	$5.19 \pm 0.08^{\mathrm{f}}$
		10	N/A	N/A	N/A	N/A
		13	N/A	N/A	N/A	N/A
	T = 70°C	7	0.092 ± 0.008^{d}	1.42 ± 0.02^{a}	90.77 ± 0.09^{a}	$5.21 \pm 0.09^{\mathrm{fg}}$
		10	$0.087 \pm 0.01^{\mathrm{a}}$	1.50 ± 0.04^{d}	91.21 ± 0.07^{de}	5.10 ± 0.14^{de}
		13	0.086 ± 0.004^{a}	1.51 ± 0.06^{de}	91.23 ± 0.10^{gh}	4.94 ± 0.04^{d}
	T = 80°C	7	0.093 ± 0.009^{c}	1.43 ± 0.11^{ab}	90.8 ± 0.09^{ab}	$5.23 \pm 0.15^{\rm h}$
		10	0.09 ± 0.006^{b}	1.44 ± 0.01^{b}	90.82 ± 0.06^{b}	$5.19 \pm 0.05^{\mathrm{f}}$
		13	0.088 ± 0.008^{ab}	1.45 ± 0.08^{c}	$91.09 \pm 0.02^{\mathrm{f}}$	$5.15 \pm 0.07^{\rm e}$
Vacuum drying	T = 60°C	7	0.092 ± 0.009^{c}	1.42 ± 0.1^{ab}	90.85 ± 0.11^{cd}	4.39 ± 0.18^{b}
		10	0.09 ± 0.012^{b}	1.43 ± 0.04^{ab}	90.97 ± 0.14^{d}	4.17 ± 0.16^{a}
		13	0.09 ± 0.007^{b}	1.43 ± 0.03^{ab}	90.99 ± 0.08^{d}	4.10 ± 0.04^{a}
	T = 70°C	7	0.092 ± 0.003^{c}	1.43 ± 0.07^{ab}	90.82 ± 0.04^{b}	4.51 ± 0.03^{bc}
		10	0.091 ± 0.004^{bc}	1.40 ± 0.09^{a}	91.08 ± 0.04^{ef}	4.47 ± 0.09^{c}
		13	0.091 ± 0.01^{bc}	1.43 ± 0.02^{ab}	90.93 ± 0.05^{d}	4.13 ± 0.07^{b}
	T = 80°C	7	0.092 ± 0.002^{e}	1.42 ± 0.04^{ab}	90.79 ± 0.04^{a}	4.82 ± 0.04^{de}
		10	0.092 ± 0.009^{c}	1.42 ± 0.12^{ab}	90.82 ± 0.11^{b}	4.56 ± 0.15^{c}
a h c d e f		13	0.09 ± 0.009^{b}	1.42 ± 0.07^{ab}	90.95 ± 0.09^{d}	4.51 ± 0.13^{c}

a, b, c, d, e, f, g in the same column with different superscripts means that the values are

significantly different (p<0.05)

N/A implies that, at this condition, the final carrot moisture content of 0.07 kg/kg (d.b.) was not achievable

Table 3. Average values of Δa and ΔL of carrot undergoing LPSSD and vacuum drying at different operating conditions.

Drying	Temperature	Pressure		A T	
Process	(°C)	(kPa)	Δa	ΔL	
LPSSD		7	$0.2 \pm 0.04^{\rm e}$	$0.01 \pm 0.02^{\mathrm{f}}$	
	$T = 60^{\circ}C$	10	N/A	N/A	
		13	N/A	N/A	
	T = 70°C	7	0.17 ± 0.02^{d}	$-0.04 \pm 0.03^{\rm e}$	
		10	0.16 ± 0.06^{d}	$-0.04 \pm 0.02^{\rm e}$	
		13	0.16 ± 0.04^{d}	$-0.04 \pm 0.04^{\rm e}$	
	T = 80°C	7	0.15 ± 0.01^{c}	-0.06 ± 0.08^{d}	
		10	0.15 ± 0.01^{c}	-0.09 ± 0.17^{abc}	
		13	0.15 ± 0.06^{c}	-0.08 ± 0.11^{cd}	
Vacuum drying	T = 60°C	7	0.10 ± 0.02^{ab}	-0.05 ± 0.03^{de}	
		10	0.10 ± 0.02^{ab}	-0.06 ± 0.03^{d}	
		13	0.09 ± 0.02^{ab}	-0.1 ± 0.08^{ab}	
	T = 70°C	7	0.07 ± 0.06^{a}	-0.09 ± 0.02^{a}	
		10	0.07 ± 0.05^{a}	-0.1 ± 0.04^{ab}	
		13	0.07 ± 0.1^{a}	-0.1 ± 0.03^{ab}	
	T = 80°C	7	0.07 ± 0.01^{a}	-0.1 ± 0.06^{ab}	
		10	0.07 ± 0.04^{a}	-0.1 ± 0.03^{ab}	
		13	0.07 ± 0.07^{a}	-0.1 ± 0.02^{ab}	

 $^{a, b, c, d, e, f}$ in the same column with different superscripts means that the values are significantly different (p<0.05)

N/A implies that, at this condition, the final carrot moisture content of 0.07 kg/kg (d.b.) was not achievable

List of Figures

- Figure 1. Schematic diagram of the overall experimental set-up
- Figure 2. Drying curves of carrot undergoing LPSSD during the first 4 hours of experiments
- Figure 3. Drying curves of carrot undergoing vacuum drying during the first 4 hours of experiments
- Figure 4. Changes in moisture content and temperature of carrot undergoing LPSSD at different operating conditions
- Figure 5. Changes in moisture content and temperature of carrot undergoing vacuum drying at different operating conditions
- Figure 6. Photographs of carrot cubes both after drying and after rehydration
- Figure 7. SEM photographs of carrot undergoing (a) LPSSD (b) vacuum drying
- Figure 8. SEM photographs showing pore distribution of carrot undergoing (a) LPSSD
 - (b) vacuum drying

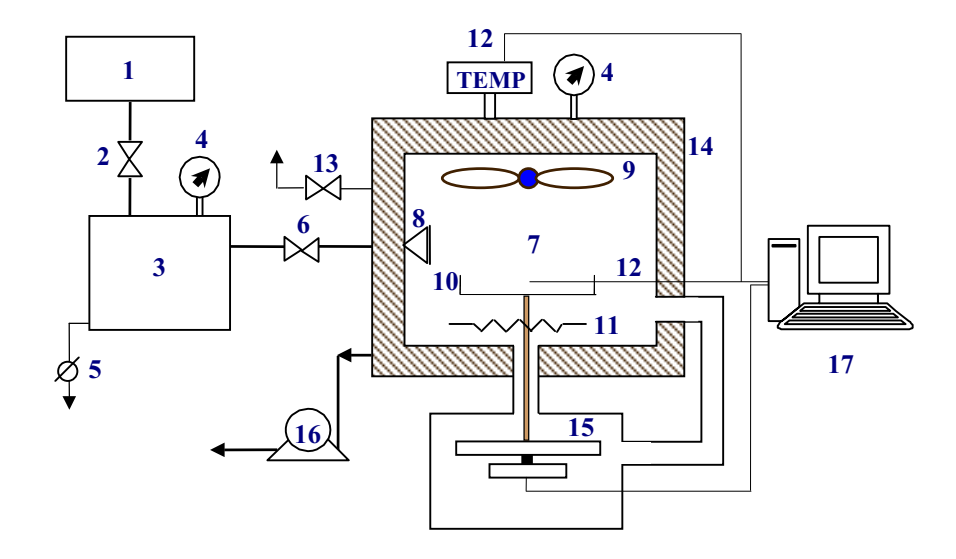


Figure 1. A schematic diagram of the low-pressure superheated steam dryer and associated units.

1, boiler; 2, steam valve; 3, steam reservoir; 4, pressure gauge; 5, steam trap; 6, steam regulator; 7, drying chamber; 8, steam inlet and distributor; 9, electric fan; 10, sample holder; 11, electric heater; 12, on-line temperature sensor and logger; 13, vacuum break-up valve; 14, insulator; 15, on-line weight indicator and logger; 16, vacuum pump; 17, PC with installed data acquisition card

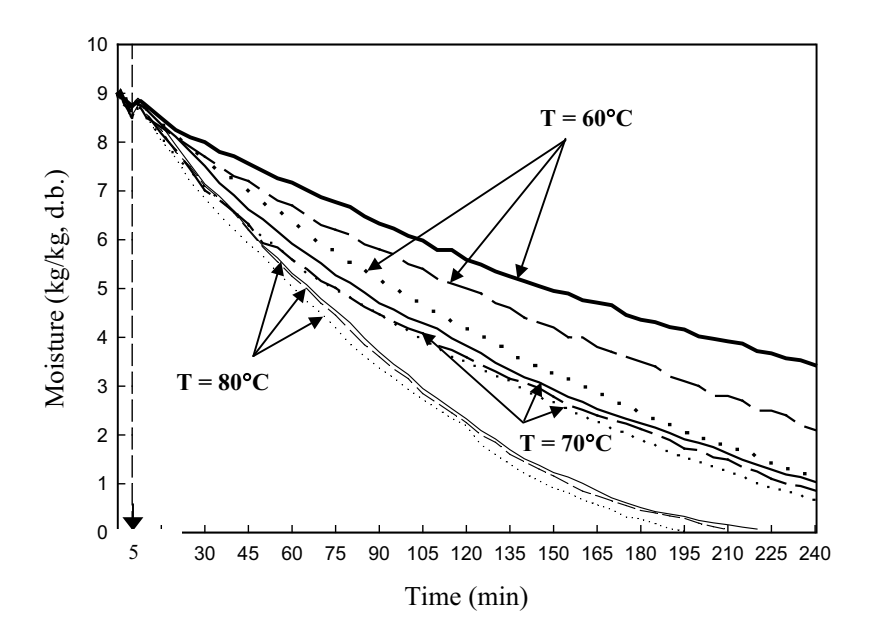


Figure 2. Drying curves of carrot undergoing LPSSD during the first 4 hours of experiments (Legends used are the same as in Figure 3).

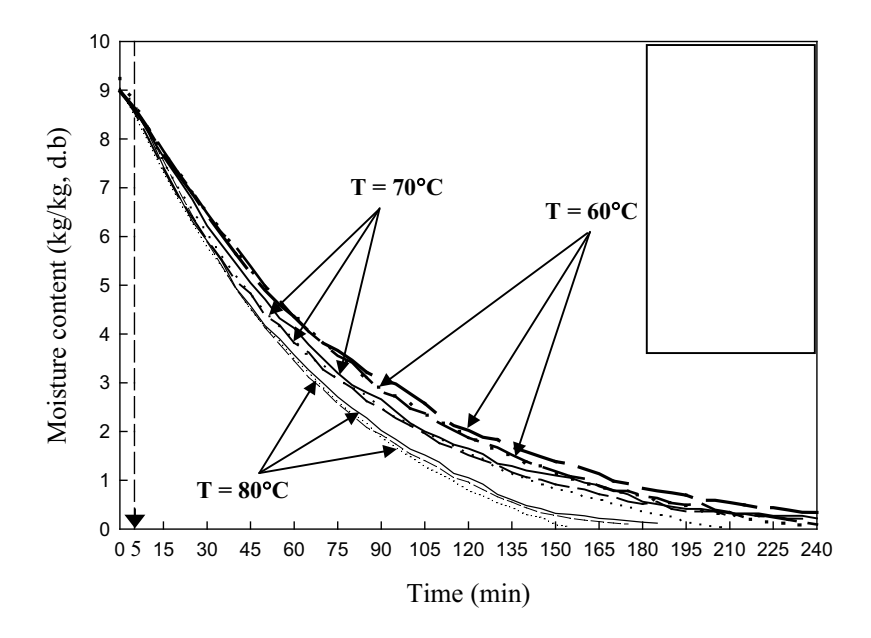


Figure 3. Drying curves of carrot undergoing vacuum drying during the first 4 hours of experiments.

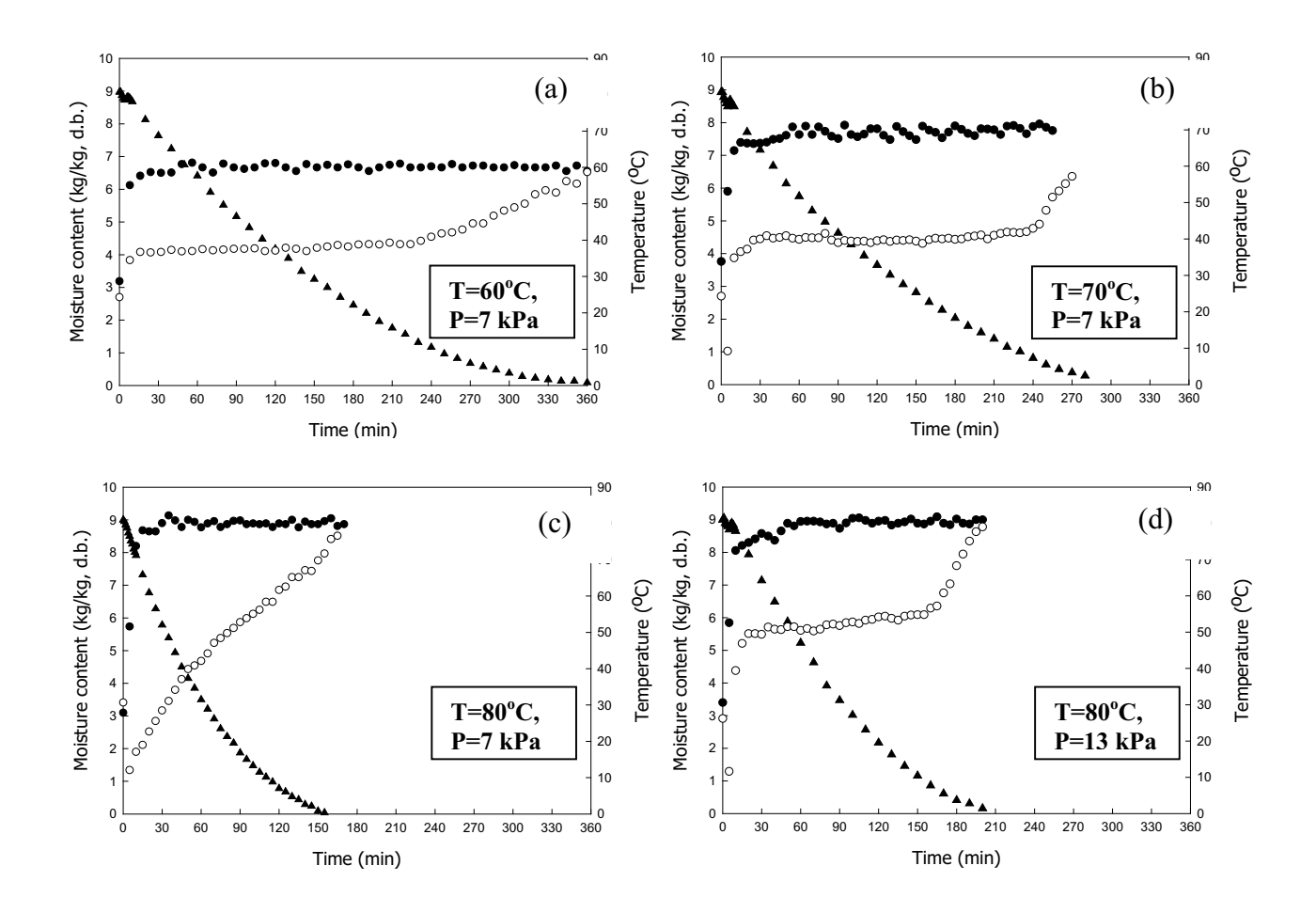


Figure 4. Changes in moisture content and temperature of carrot undergoing LPSSD at different operating conditions. ▲ moisture content; ● steam temperature; ○ sample temperature

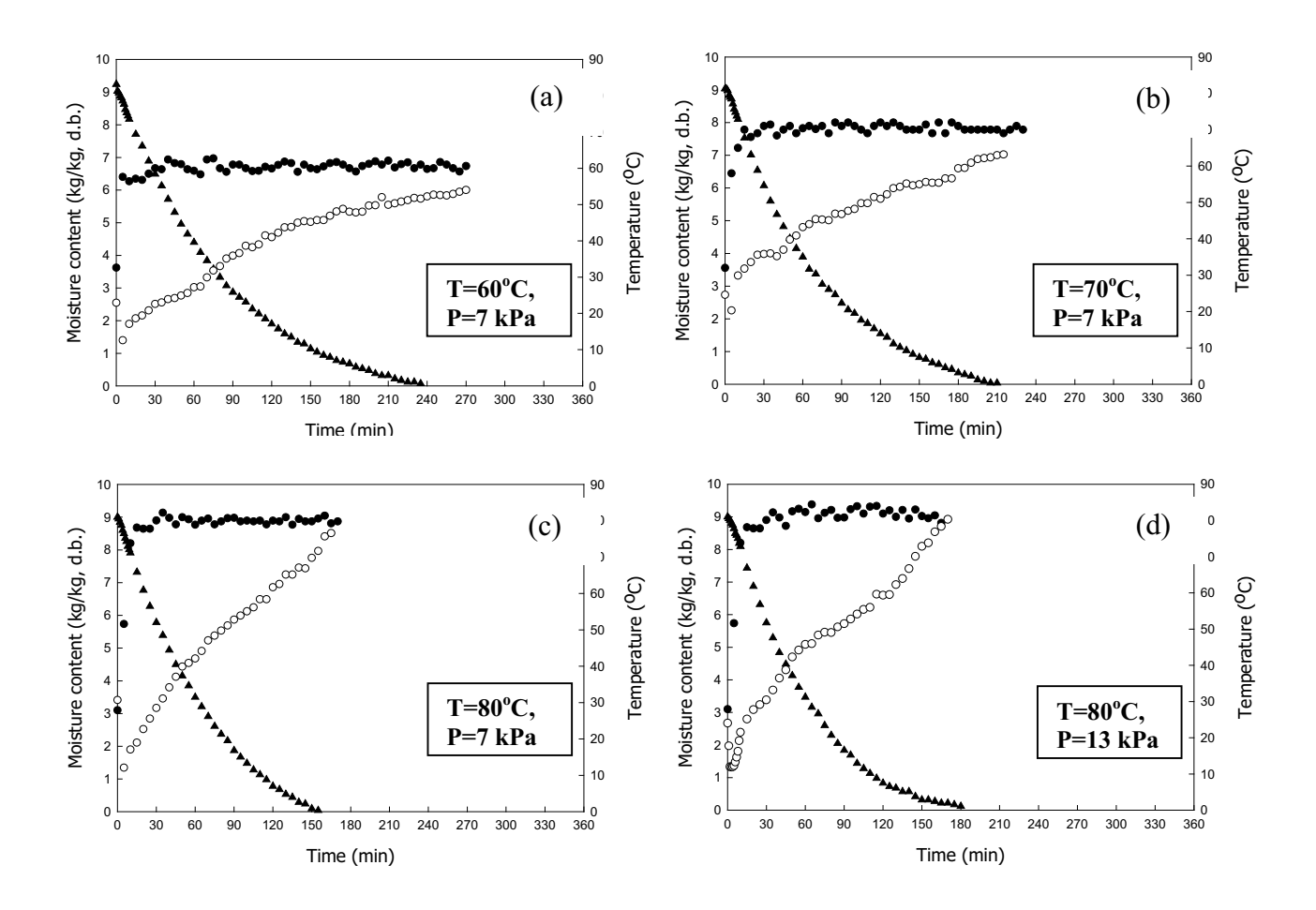


Figure 5. Changes in moisture content and temperature of carrot undergoing vacuum drying at different operating conditions. ▲ moisture content; ● steam temperature; o sample temperature

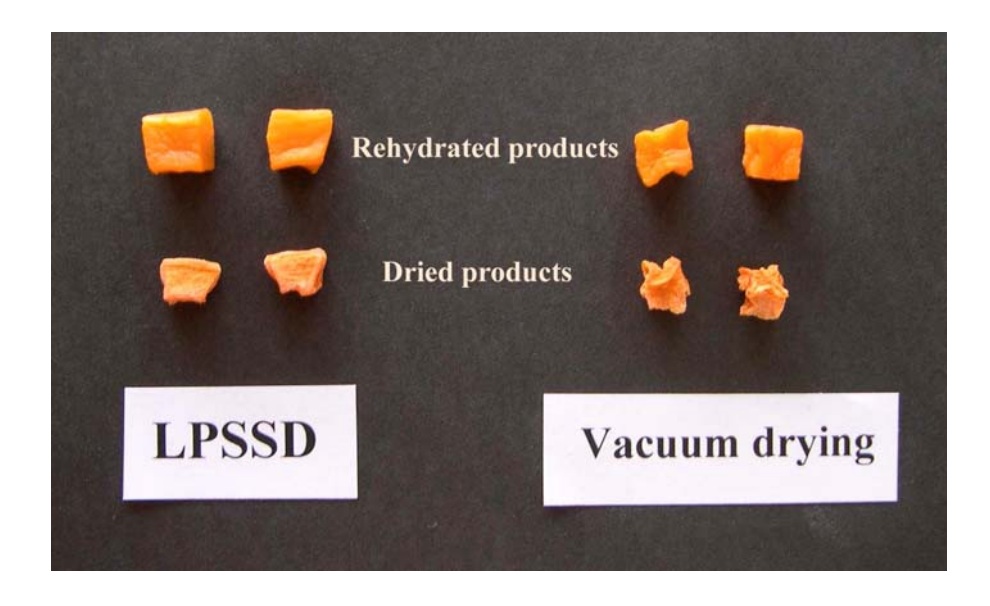
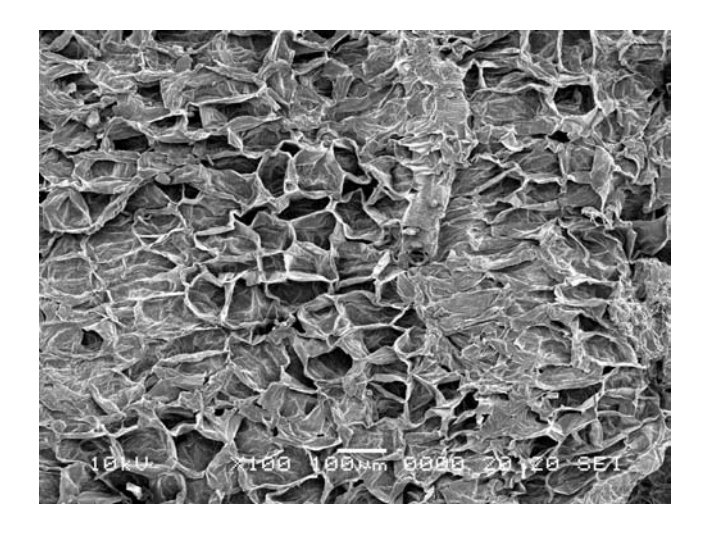


Figure 6. Photographs of carrot cubes both after drying and after rehydration



(a)

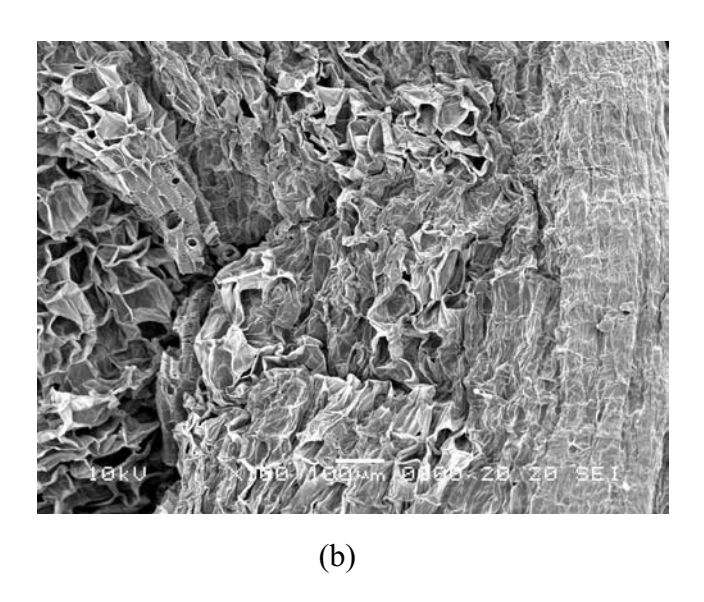


Figure 7. SEM photographs of carrot undergoing

(a) LPSSD

(b) Vacuum drying



(a)

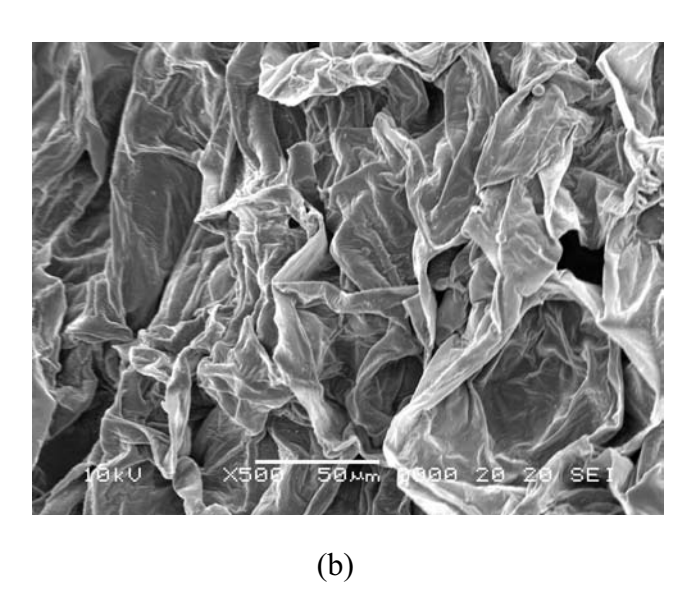


Figure 8. SEM photographs showing pore distribution of carrot undergoing

(a) LPSSD

(b) Vacuum drying

The 15th International Symposium on Transport Phenomena, 9-13 May 2004, Bangkok, Thailand

Appendix 2

DRYING RATES AND INVERSION TEMPERATURES OF POROUS PARTICLES UNDERGOING LOW-PRESSURE SUPERHEATED STEAM AND VACUUM DRYING

P. Suvarnakuta^{1,*}, S. Devahastin¹, S. Soponronnarit² and A.S. Mujumdar³

¹Department of Food Engineering, ²School of Energy and Materials King Mongkut's University of Technology Thonburi, Bangkok 10140, Thailand ³Department of Mechanical Engineering, National University of Singapore, Singapore 117576

ABSTRACT

The present study aimed at investigating the drying rates and inversion temperatures of model porous particles undergoing low-pressure superheated steam and vacuum drying. Molecular sieve beads, which were used as the model material in this work, were dried as a thin layer in a newly developed low-pressure superheated steam dryer. The effects of various operating conditions viz. steam temperature and pressure on the drying rates of these particles were then determined. The same dryer was also operated in a vacuum mode, but without the application of low-pressure superheated steam, to determine the effects of the above-mentioned operating parameters as well as the variation of the inversion temperature of the processes with the operating pressure. The differences between the values of the inversion temperature calculated from the rates of drying in the constant rate period and those calculated from the whole drying period were also pointed out and discussed.

Keywords: constant rate period drying, molecular sieve, pressure, thin-layer drying

INTRODUCTION

Despite the many advantages of near-atmospheric pressure superheated steam drying, there still exist some limitations, especially when applying it to drying heat-sensitive materials, e.g., foods and bio-products [1]. Since most foods or other heat-sensitive products melt, undergo glass transition or are damaged at the saturation temperature of superheated steam corresponding to the atmospheric or higher pressures, one possible way to alleviate the abovementioned problems is to operate the dryer at reduced pressure [1, 2, 3]. In addition to being able to preserve the quality of heat-sensitive products, lowering the operating pressure may also enhance the drying rates as well [1, 4, 5, 6, 7, 8].

Several investigators have recently applied the concept of low-pressure (or vacuum or sub-atmospheric pressure) superheated steam drying to dry various types of heatsensitive materials. Elustondo et al. [3] studied subatmospheric pressure superheated steam drying of wood slabs, shrimps, bananas, apples, potatoes and cassava slices both experimentally and theoretically. A semi-empirical model was developed assuming that the water removal was carried out by evaporation in a moving boundary allowing the vapor to flow through the dry layer built as drying proceeded to predict the drying characteristics of material undergoing this drying operation. A model proposed was found to predict the drying kinetics reasonably well. More recently, Devahastin et al. [9] studied experimentally drying of carrot cubes both in low-pressure superheated steam and vacuum dryers. They observed that the differences between the two sets of drying times (belonged to low-pressure superheated steam and vacuum drying) were smaller at higher drying temperature. This suggested that raising the drying temperature farther would eventually lead to equal rates of drying at the so-called inversion temperature [1] due to increased temperature difference between the steam and the product as well as a reduction of the initial steam condensation. The information on inversion temperature and the effect of vacuum pressure on this temperature was still missing, however.

The present work therefore aimed at investigating the effect of the vacuum pressure on the value of inversion temperature when comparing the thin-layer drying rates of the low-pressure superheated steam and vacuum drying of model porous particles viz. molecular sieve beads. In addition, the values of the inversion temperature calculated only from the rates of drying in the constant rate period were compared with those calculated from the whole drying period (constant rate period and falling rate period) in order to point out the fundamental difference between the two sets of temperatures, obtained from two different sets of drying rates, beyond which the drying rates in low-pressure superheated steam drying were higher than those in vacuum drying.

EXPERIMENTAL SET-UP, MATERIAL AND METHODS

Experimental Set-up

A schematic diagram of the low-pressure superheated steam dryer and its accessories is shown in Figure 1. The dryer consists of a stainless steel drying chamber, insulated carefully with rock wool, with an inner dimension of 45×

Tel: +662 470 9340; Fax: +662 470 9240; e-mail: peamsuk s@hotmail.com

^{*} Corresponding author.

45×45 cm³; a steam reservoir, which received steam from the boiler and maintained its pressure at around 200 kPa (gage); and a liquid ring vacuum pump (Nash, model ET32030, Germany), which was used to maintain the vacuum in the drying chamber. Steam trap was installed to reduce the excess steam condensation in the reservoir. An electric heater, rated at 1.5 kW, which was controlled by a PID controller (Omron, model E5CN, Japan) was installed in the drying chamber to control the steam temperature and to minimize the condensation of steam in the drying chamber during the start-up period; with the use of a heater the initial steam condensation during the start-up period was reduced considerably. A variable-speed electric fan was used to disperse steam throughout the drying chamber. The steam inlet was made into a cone shape and was covered with a screen to also help distributing the steam in the chamber. The sample holder was made of a stainless steel screen with a dimension of 12×12 cm². The change of the weight of the sample was detected continuously (at 1 minute intervals) using a load cell (Minebea, model Ucg-3kg, Japan), which was installed in a smaller chamber connected to the drying chamber by a flexible hose (in order to maintain the same vacuum pressure as that in the drying chamber), and also to an indicator and recorder (AND A&D Co., model AD 4329, Japan). The temperature of the steam measured continuously was also using type thermocouples, which were connected to an expansion board (Omega Engineering, model no. EXP-32, USA). Thermocouple signals were then multiplexed to a data acquisition card (Omega Engineering, model no. CIO-DAS16Jr., USA) installed in a PC. LABTECH NOTEBOOK software (version 12.1, Laboratory Technologies Corp., USA) was then used to read and record the temperature data.

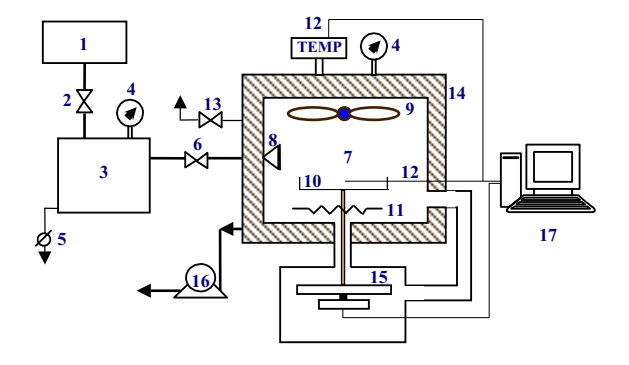


Figure 1. A schematic diagram of the low-pressure superheated steam dryer and associated units. 1, boiler; 2, steam valve; 3, steam reservoir; 4, pressure gauge; 5, steam trap; 6, steam regulator; 7, drying chamber; 8, steam inlet and distributor; 9, electric fan; 10, sample holder; 11, electric heater; 12, on-line temperature sensor and logger; 13, vacuum break-up valve; 14, insulator; 15, on-line weight

indicator and logger; 16, vacuum pump; 17, PC with installed data acquisition card

Material and Methods

Molecular sieve beads, which have pore size of 0.3 nm and an average diameter of 3.02 mm with the standard deviation of 0.34 mm and bulk density of 750 kg/m³ were used as the tested material in this work. Prior to the start of each experiment, distilled water (6.7 g) was added to beads (22 g) to make the initial moisture content of the beads to be around 0.3 kg/kg (d.b.), which was roughly the maximum moisture holding capacity of the beads. The particles were then left at room temperature for about 5 hours to allow them to reach the equilibrium. The drying experiment was preformed by placing roughly 28.7 g of saturated particles (about 1000 beads) on the sample holder as a thin layer. The drying chamber was then sealed tightly and valve 2 was opened to allow the steam from the boiler to flow into the reservoir; the steam pressure was maintained at about 200 kPa (gage) in the reservoir. A vacuum pump was then switched on to evacuate the drying chamber to the desired operating pressure and the steam regulator was opened to slowly flash the steam into the drying chamber. Due to the low-pressure environment of the chamber the steam became superheated. An electric heater was used to maintain the steam temperature at a desired drying temperature. At the end of the drying process the break-up valve was opened to allow the air into the drying chamber before opening up the chamber door and loading off the samples.

The experiments were performed at the following conditions: steam absolute pressures of 7, 10 and 13 kPa; steam temperatures of 80°, 90° and 100°C. The flow rate of steam into the drying chamber was maintained at about 26 kg/h and the speed of the fan was fixed at 2100 rpm.

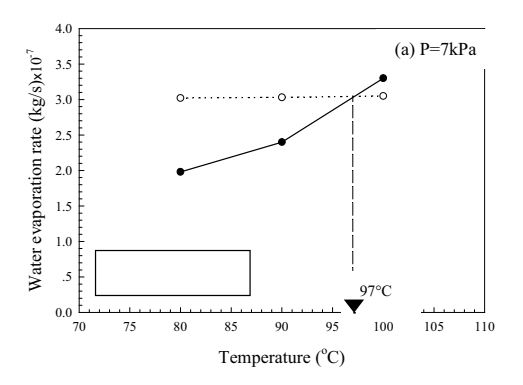
For vacuum drying experiments the same experimental set-up was used but without the application of steam to the drying chamber. The same operating conditions were therefore achievable.

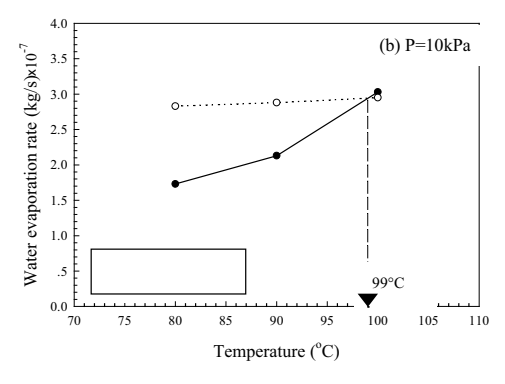
RESULTS AND DISCUSSION

Drying rates of porous particles

Molecular sieve beads, which were saturated with moisture (initial moisture content about 0.3 kg/kg (d.b.) or 23% (w.b.)), were dried to their equilibrium moisture content at each operating condition in the dryer using both low-pressure superheated steam and vacuum conditions. At the end of each experiment the drying rates were calculated from the recorded weight changes, both during the constant and falling rate periods. Since, strictly speaking, the inversion temperature is defined only for surface moisture evaporation and not for internal moisture removal, the drying rates belonged to the constant rate period would first be reported. The average drying rates, based on the rates both in the constant and falling rate periods, were then calculated and compared with the rates in the constant rate

period to point out the fundamental differences between the values of the inversion temperatures calculated using only the rates in the constant rate period and those obtained using the average drying rate in both drying periods.





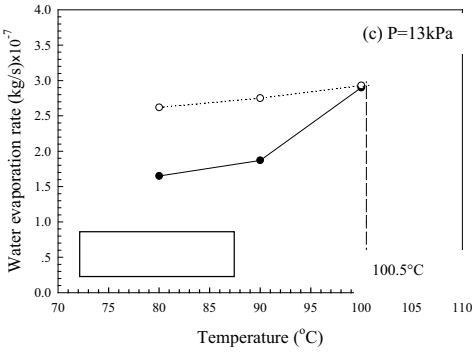


Figure 2. Constant-rate period evaporation rates of moisture from molecular sieve beads at various operating pressures.

Figure 2 shows the rates of water evaporation in the constant rate period at various operating temperatures and pressures. It was found, as expected, that raising the drying temperature led to higher constant rate period (CRP) drying rates due to increased temperature difference or gradient between the steam (or air) and the samples as well as a reduction of the initial steam condensation in the case of superheated steam drying. In the case of low-pressure superheated steam drying, the temperature difference was the difference between the superheated steam and saturation

temperature at the corresponding operating pressure, while the temperature difference was the difference between the air and wet bulb temperatures in the case of vacuum drying. While the temperature differences (or driving force for heat transfer) of vacuum drying were higher at lower operating temperatures than those of low-pressure superheated steam drying, the values of the heat transfer coefficient were lower due to inferior thermal properties of air. Raising the drying temperature, however, led to higher temperature differences and hence higher CRP drying rates. The counter-acting effects of the heat transfer coefficient and temperature difference led to inversion phenomenon, as shown also in Figure 2, where the CRP drying rates of vacuum drying and low-pressure superheated steam drying were equal. Beyond the inversion temperature the CRP drying rates of steam drying were higher than those of vacuum drying due both to the increased temperature differences and higher heattransfer coefficients.

When the operating pressure increased (at the same operating temperature) it can be seen that the evaporation rate was lower. This was due to the fact that the boiling temperature of water at higher pressure is higher; this led to decreased temperature difference and hence lower water evaporated rate.

As mentioned earlier, the CRP drying rates depend on the rate of heat transfer and hence the difference between the surface temperature of the sample and the drying medium temperature. For this reason, the drying temperature had only a small effect on the rates of vacuum drying as compared with the case of low-pressure superheated steam dying since the wet-bulb temperature changes only slightly with increased drying temperature compared with the change of boiling temperature, especially at lower operating pressures.

Inversion temperature

Figure 3 shows the effect of operating pressure on the inversion temperature, which was calculated from the CRP rates (Figure 2). The inversion temperature at the operating pressure of 13 kPa was obtained by extending the plots of drying rates to the point where rates of vacuum and lowpressure superheated steam were equal. The data here confirm that the inversion temperature depends on the operating pressure and correlates almost linearly with the operating pressure. This is because water at the surface of particles evaporates faster at lower pressures than at higher pressures because the difference between the boiling point and superheated steam temperature was higher as mentioned earlier. It is seen also from Figure 3 that when steam drying was performed at lower operating pressures (less than 7 kPa), its CRP drying rate would be higher than that of vacuum drying even at temperatures lower than 97°C. Using these conditions to operate the dryer would yield shorter drying times and this might preserve the quality of the product better.

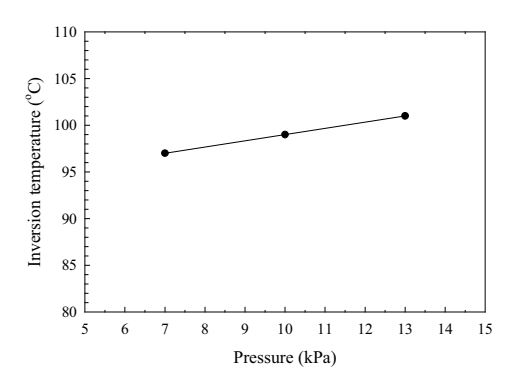


Figure 3. Effect of operating pressure on inversion temperature (based on CRP drying rates) of molecular sieve beads.

Figure 4, on the other hand, shows the average drying rates calculated from combined constant rate period (CRP) and falling rate period (FRP) drying rates when using the operating pressure of 7 kPa. The intersection point was obtained by extending the plots of drying rates to the point where rates of vacuum and low-pressure superheated steam drying were equal. As mentioned earlier, the CRP drying rates depend only on external heat and mass transfer conditions since free water is always available for evaporation at the surface of the samples. However, in the FRP the rates depend not only on the rate of external heat transfer but more on the internal resistances to heat and mass transfer, which are somewhat material-dependent. Therefore, the inversion temperature calculated from combined CRP and FRP rates (or temperature at the intersection point, 113°C) was not equal to that calculated from only CRP drying rates. It can also be seen from Figure 2 (a) and Figure 4 that the differences between vacuum and steam drying rates calculated only from CRP rates were greater than those between vacuum and steam drying calculated from combined CRP and FRP rates. This is due to the fact that in FRP the resistances of heat and mass transfer of superheated steam drying were lower than those of vacuum drying because the drying medium of steam drying was water. These effects of FRP drying rates therefore increased the values of the combined (or overall) drying rates of superheated steam drying and hence led to smaller differences between the overall drying rates of vacuum and steam drying.

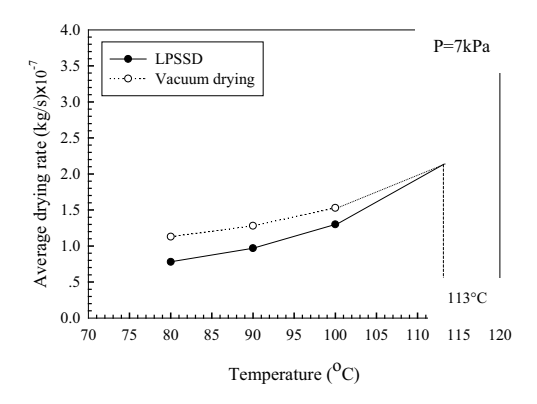


Figure 4. Average rate of moisture removal from molecular sieve beads at an operating pressure of 7 kPa.

In addition, it can be seen from Figure 4 that the inversion temperature calculated from combined CRP and FRP rates (113°C) was higher than the inversion temperature calculated from only CRP rates (97°C). This is because towards the end of FRP of low-pressure superheated steam drying the drying rates were lower than those of vacuum drying since the equilibrium moisture content of particles in low-pressure superheated steam environment was higher and hence lower driving force for moisture transfer. This is due to the fact that the drying chamber had higher humidity values than the drying chamber of vacuum drying. For example, the equilibrium moisture contents of particles dried at 80°, 90° and 100°C using low-pressure superheated steam drying were 0.8, 0.5 and 0.2% (d.b.), respectively, at the operating pressure of 7 kPa. At higher operating pressures (say, 13 kPa) the moisture contents of particles dried in a low-pressure superheated steam dryer were even higher and these led to the reduction of the combined rates of drying of the lowpressure superheated steam drying. Therefore, at higher operating pressures the intersection points of equal rates of drying might not even be obtainable (data not shown for the sake of brevity).

CONCLUSION

Effects of operating parameters, i.e., drying temperature and pressure, on the rates of vacuum and low-pressure superheated steam drying of model porous particles were experimentally investigated in this study. In addition, the values of the inversion temperature calculated only from the rates of drying in the constant rate period were compared with those calculated from the whole drying period (constant rate period and falling rate period) in order to point out the fundamental difference between the two sets of temperatures beyond which the drying rates in low-pressure superheated steam drying were higher than those in vacuum drying. It was found that the inversion temperature

calculated from combined CRP and FRP rates was higher than the inversion temperature calculated from only CRP rates. At higher operating pressures the intersection points of equal rates of drying might not even be obtainable.

ACKNOWLEDGEMENTS

The authors would like to express their sincere appreciation to the Thailand Research Fund (TRF) and the International Foundation for Science (Sweden) for supporting this study financially.

REFERENCES

- 1. A.S. Mujumdar, Superheated steam drying technology of the future, In *Mujumdar's Practical Guide to Industrial Drying*, S. Devahastin, Ed. Exergex, Brossard, Canada (2000).
- 2. P. Kumar, A.S. Mujumdar, Superheated-steam drying: a bibliography, *Drying Technology* 8, 1 (1990).
- 3. D. Elustondo, M.P. Elustondo, M.J. Urbicain, Mathematical modeling of moisture evaporation from foodstuffs exposed to subatmospheric pressure superheated steam, *Journal of Food Engineering* 49, 1 (2001).
- 4. H. Shibata, J. Mada, H. Shinohara, Drying mechanism of sintered spheres of glass beads in superheated steam, *Industrial & Engineering Chemistry Research* 27, 12 (1988).
- 5. H. Shibata, J. Mada, K. Funatsu, Prediction of drying curves on sintered spheres of glass beads in superheated steam under vacuum, *Industrial & Engineering Chemistry Research* 29, 4 (1990).
- Y. Senda, Y. Bando, K. Yasuda, M. Nakamura, Y. Sugimura, M. Shibata, Development of superheated steam dryer at reduced pressure, In *Proceeding of the 1st Asia -Pacific Drying Conference*, Bali, Indonesia (2001).
- 7. D.M. Elustondo, A.S. Mujumdar, M.J. Urbicain, Optimum operating conditions in drying foodstuffs with superheated steam, *Drying Technology* 20, 2 (2002).
- 8. D. Elustondo, M.P. Elustondo, M.J. Urbicain, Drying with superheated steam: maximum drying rate as a linear function of pressure, *Chemical Engineering Journal* 86, 1-2 (2002).
- 9. S. Devahastin, P. Suvarnakuta, S. Soponronnarit, A.S. Mujumdar, A comparative study of low-pressure superheated steam and vacuum drying of a heat-sensitive material, [*In press*], *Drying Technology* (2004).



Drying Kinetics and Inversion Temperature in a Low-Pressure Superheated Steam Drying System

P. Suvarnakuta¹, S. Devahastin^{1,*}, S. Soponronnarit² and A.S. Mujumdar³

¹Department of Food Engineering, ²School of Energy and Materials

King Mongkut's University of Technology Thonburi, Bangkok 10140, Thailand

³Department of Mechanical Engineering, National University of Singapore, Singapore 117576

Tel: +662 470 9246; Fax: +662 470 9240; e-mail: sakamon.dev@kmutt.ac.th

^{*} Corresponding author.

Abstract

The present study is aimed at investigating the drying rates and inversion temperatures for model porous particles undergoing low-pressure superheated steam and vacuum drying. Molecular sieve beads, which were used as the model material in this work, were dried as a thin layer in a low-pressure superheated steam dryer. The effects of various operating parameters viz. steam temperature and pressure on the drying rates of these particles were determined. The same dryer was also operated in a vacuum mode to determine the effects of the above-mentioned operating parameters as well as the variation of the inversion temperature of the processes with the operating pressure. The differences between the values of the inversion temperature calculated only from the rates of drying in the constant rate period and those calculated from the whole drying period are pointed out and discussed. Page's equations and a single-term exponential equation were found to satisfactorily describe the kinetics of low-pressure superheated steam drying and vacuum drying system, respectively.

Key words and phrases: constant rate period drying, empirical models, falling rate period drying, molecular sieve, thin-layer drying

Introduction

Despite the many advantages of near-atmospheric pressure superheated steam drying, there still exist some limitations, especially when applying it to drying heat-sensitive materials, e.g., foods and bio-products.¹ Since most foods or other heat-sensitive products melt, undergo glass transition or are damaged at the saturation temperature of superheated steam corresponding to the atmospheric or higher pressures, one possible way to alleviate the above-mentioned problems is to operate the dryer at reduced pressure.¹⁻³ In addition to being able to preserve the quality of heat-sensitive products, lowering the operating pressure may also enhance the drying rates as well.^{1,4,5-8}

Some investigators have recently applied the concept of low-pressure (or sub-atmospheric pressure) superheated steam drying to various heat-sensitive materials. Elustondo et al.³ studied sub-atmospheric pressure superheated steam drying of wood slabs, shrimp, banana, apple, pear, potato and cassava slices both experimentally and theoretically. A semi-empirical model was developed assuming that the water removal was accomplished by evaporation in a moving boundary allowing the vapor to flow through the dry layer built up as drying proceeds. The model proposed was found to predict the drying kinetics reasonably well. More recently, Devahastin et al. 9 studied experimentally drying of carrot cubes both in low-pressure superheated steam and vacuum dryers. They observed that the differences between the two sets of drying (low-pressure superheated steam and vacuum drying) were smaller at higher drying temperatures. This suggested that raising the drying temperature further would eventually lead to equal rates of drying at the so-called inversion temperature due to increased temperature difference between the steam and the product as well as due to a reduction in the initial steam condensation that occurs as the wet material enters the drying chamber at a temperature lower than the saturation temperature of steam at prevailing pressure. Such information on the inversion temperature for the low-pressure superheated steam drying system and the effect of vacuum pressure on this temperature is still missing, however. Although Shibata et al.⁴ and Shibata et al.¹⁰ have, respectively, studied the steam drying mechanisms of sintered spheres of glass beads under atmospheric pressure and vacuum. They reported that the drying mechanisms in the two processes were different and that superheated steam drying under vacuum gave lower critical moisture contents as well as higher drying rates in the falling rate period than those in air drying under vacuum, they have not reported any information about the inversion temperature of the systems.

The present work therefore is aimed at investigating the effect of vacuum pressure on the value of inversion temperature by comparing the thin-layer drying rates obtained in low-pressure superheated steam drying (LPSSD) and in vacuum drying of model porous particles viz.

molecular sieve beads. In addition, the values of the inversion temperatures calculated only from the rates of drying in the constant rate period were compared with those calculated from the whole drying period (constant rate period and falling rate period) in order to point out the fundamental differences between the two sets of temperatures, obtained from two different sets of drying rate information, beyond which drying rates in low-pressure superheated steam drying are higher than those in vacuum drying. Three simple mathematical models that enable prediction of the drying behavior of molecular sieves undergoing LPSSD and vacuum drying are also proposed and compared.

Experimental Set-up, Material and Methods

Experimental Set-up

A schematic diagram of the low-pressure superheated steam dryer and its accessories is shown in Figure 1. The dryer consists of a stainless steel drying chamber, insulated carefully with rock wool, with inner dimensions of 45×45×45 cm³; a steam reservoir, which received steam from the boiler and maintained its pressure at around 200 kPa (gage); and a liquid ring vacuum pump (Nash, model ET32030, Germany), which was used to maintain vacuum in the drying chamber. A steam trap was installed to reduce excess steam condensation in the reservoir. An electric heater, rated at 1.5 kW, controlled by a PID controller (Omron, model E5CN, Japan), was installed in the drying chamber to control the steam temperature and to minimize condensation of steam in the drying chamber during start-up; with the use of a heater the initial steam condensation during the start-up period was reduced considerably. A variable-speed electric fan was used to disperse steam well throughout the drying chamber. The steam inlet was made into a conical shape and was covered with a screen to help distribute the steam in the chamber. The sample holder was made of a stainless steel screen with dimensions of 12×12 cm². The change of the mass of the sample was detected continuously (at 1 minute intervals) using a load cell (Minebea, model Ucg-3kg, Japan), which was installed in a smaller chamber connected

to the drying chamber by a flexible hose (in order to maintain the same vacuum pressure as that in the drying chamber), and also to an indicator and recorder (AND A&D Co., model AD 4329, Japan). The temperature of the steam was also measured continuously using type K thermocouples, which were connected to an expansion board (Omega Engineering, model no. EXP-32, USA). Thermocouple signals were then multiplexed to a data acquisition card (Omega Engineering, model no. CIO-DAS16Jr., USA) installed in a PC. LABTECH NOTEBOOK software (version 12.1, Laboratory Technologies Corp., USA) was used to read and record the temperature data.

Material and Methods

Molecular sieve beads (Fluka, No. 69837), which have a pore size of 0.4 nm and an average diameter of 3.02 mm with a standard deviation of 0.34 mm and bulk density of 750 kg/m³ were used as test material in this work. Prior to the start of each experiment, distilled water (6.7 g) was slowly but continuously sprayed on to the beads (22 g) to make the initial moisture content of the beads to be around 0.3 kg/kg (d.b.), which was roughly the maximum moisture holding capacity of the beads. The particles were then left in a tightly closed box at room temperature for about 5 hours to allow them to reach equilibrium. The drying experiment was performed by placing roughly 28.7 g of water-saturated particles (about 1000 beads) on the sample holder as a thin layer. The drying chamber was then sealed tightly and valve 2 was opened to allow the steam from the boiler to flow into the reservoir; the steam pressure was maintained at about 200 kPa (gage) in the reservoir. A vacuum pump was then switched on to evacuate the drying chamber to the desired operating pressure and the steam regulator was opened to slowly flash the steam into the drying chamber. Due to the low-pressure environment in the chamber the steam became superheated. An electric heater was used to maintain the steam temperature at the desired drying temperature. At the end of drying the break-up valve was

opened to allow the air into the drying chamber before opening up the chamber door and loading off the sample.

The experiments were performed under the following conditions: steam absolute pressures of 7, 10 and 13 kPa; steam temperatures of 80°, 90° and 100°C. The flow rate of steam into the drying chamber was maintained at about 26 kg/h and the speed of the fan was fixed at 2100 rpm.

For vacuum drying experiments the same experimental set-up was used but without the application of steam to the drying chamber. The same operating conditions as those used for LPSSD were therefore achievable.

Results and Discussion

Drying rates of porous particles

Molecular sieve beads, which were saturated with water (initial moisture content was about 0.3 kg/kg (d.b.) or 23% (w.b.)), were dried to their equilibrium moisture content at each operating condition in the dryer using both low-pressure superheated steam and vacuum conditions. During each experiment the drying rates were calculated from the recorded weight changes, both during the constant and falling rate periods. Since, strictly speaking, the inversion temperature is defined only for surface moisture evaporation and not for internal moisture removal, the drying rates in the constant rate period (CRP) are reported first. The overall average drying rates, based on the rates both in the constant and falling rate periods, were then calculated and compared with the rates in the constant rate period to point out the fundamental differences between the values of the inversion temperatures calculated using only the rates in the constant rate period and those obtained using the overall average drying rates in both drying periods.

First, the drying curves for the thin-layer of particles undergoing LPSSD and vacuum drying at some selected conditions are shown in Figure 2. The drying curves for LPSSD at different conditions were quite different; also, the effect of temperature on the drying curves was greater than the effect of pressure, while the drying curves for vacuum drying at different

operating conditions were rather similar. It is seen that the drying times of LPSSD at an operating temperature of 80°C were longer than those of vacuum drying for all operating pressures tested. However, the drying times for both processes operated at 100°C were quite similar. This is due to the fact that increased drying temperature led to higher drying rates resulting from sharply increased temperature differences or gradients between the samples and the ambient steam in the case of superheated steam drying. However, the temperature differences between the air temperature and the wet-bulb temperature in vacuum drying increased only slightly as the drying temperature increased. In addition, it can be observed that the equilibrium moisture contents of the beads undergoing LPSSD were much higher than those undergoing vacuum drying. For example, the equilibrium moisture contents of particles dried at 80°, 90° and 100°C using LPSSD at an operating pressure of 7 kPa were 1.5, 0.9 and 0.2% (d.b.), respectively, while the equilibrium moisture contents of particles were 0.09, 0.05, 0.02% (d.b.), respectively, in the case of vacuum drying at the same pressure. This led to increased humidity in the drying chamber of LPSSD and hence reduced the vapor pressure gradient, which is the driving force of the drying process. Therefore, the drying times of most LPSSD were higher than those of vacuum drying.

Figure 3 shows a comparison of the observed drying rate curves in superheated steam drying with those in vacuum drying at different operating conditions. For all conditions the drying rates fluctuated marginally but remained nearly constant as the moisture content decreased until the critical moisture content for each condition was reached. The drying rates then decreased continuously in the falling rate period (FRP). It can be seen from this figure that the critical moisture content was different for different conditions in the case of superheated steam drying (the critical moisture contents of particles dried, for example, at 80°, 90° and 100°C were 20, 17 and 15% (d.b.), respectively, at the operating pressure of 7 kPa), but were quite similar in the case vacuum drying (17% (d.b.) over the temperature range of 80°- 100°C at the

operating pressure of 7 kPa). It was also observed that the lower-pressure and higher-temperature superheated steam led to larger amount of water evaporation and also to higher critical moisture contents.

Figure 4 gives the rates of water evaporation during the constant rate period at various operating temperatures and pressures. It was found, as expected, that raising the drying temperature led to higher CRP drying rates due to increased temperature difference between the steam (or air) and the samples as well as a reduction of the initial steam condensation in the case of superheated steam drying. In the case of low-pressure superheated steam drying, the temperature difference was the difference between the superheated steam and saturation temperature at the corresponding operating pressure, while the temperature difference was the difference between the air temperature and the wet-bulb temperature (not saturation temperature since, in this case, the level of vacuum was not that high that the effect of convection by the fan could be negligible) in the case of vacuum drying. While the temperature differences (or driving force for heat transfer) in vacuum drying were higher at lower operating temperatures than those observed in low-pressure superheated steam drying, the values of the heat transfer coefficient were lower due to the inferior thermal properties of air. Raising the drying temperature, however, led to higher temperature differences and hence higher CRP drying rates. The counter-acting effects of the heat transfer coefficient and the temperature difference lead to the inversion phenomenon, as is evident in Figure 4, where the CRP drying rates of vacuum drying and lowpressure superheated steam drying are seen to be equal. Beyond the inversion temperature the CRP drying rates of steam drying were higher than those of vacuum drying due both to the increased temperature difference and higher heat transfer coefficient.

When the operating pressure increased (at the same operating temperature) it can be seen that the evaporation rate was lower. This was due to the fact that the boiling temperature of water at higher pressure is higher; this leads to decreased temperature difference and hence lower water evaporated rate.

As mentioned earlier, the CRP drying rates depend on the rate of heat transfer and hence the difference between the surface temperature of the sample and the drying medium temperature. For this reason, the drying temperature had only a small effect on the rates of vacuum drying as compared with the case of low-pressure superheated steam dying since the wet-bulb temperature changes only slightly with increased drying temperature compared with the change of boiling temperature, especially at lower operating pressures.

Inversion temperature

Figure 5 shows the effect of operating pressure on the inversion temperature, which was calculated from the CRP rates (Figure 4). The inversion temperature at the operating pressure of 13 kPa was obtained by extending the plots of drying rates to the point where rates of vacuum and low-pressure superheated steam drying were equal. The data here confirm that the inversion temperature depends on the operating pressure and correlates almost linearly with it. This is because water at the surface of particles evaporates faster at lower pressures than at higher pressures because the difference between the boiling point and superheated steam temperature was higher as mentioned earlier. It is seen also from Figure 5 that when steam drying was performed at lower operating pressures (less than 7 kPa), its CRP drying rate would be higher than that of vacuum drying even at temperatures lower than 93°C. Using these conditions to operate the dryer would yield shorter drying times and this might preserve the quality of a heat-sensitive product better.

Figure 6, on the other hand, shows the overall average drying rates calculated from combined constant rate period and falling rate period drying rates at various operating pressures. The intersection point was obtained by extending the plots of drying rates to the point where rates of vacuum and low-pressure superheated steam drying were equal. As mentioned earlier, the CRP drying rates depend only on external heat and mass transfer conditions since free water is always available for evaporation at the surface of the sample. However, in the FRP the rates

depend not only on the rate of external heat transfer but more on the internal resistances to heat and mass transfer, which are somewhat material-dependent. Therefore, the inversion temperatures calculated from combined CRP and FRP rates (or temperature at the intersection point, in the case where P = 7ka, 109°C) were not the same as those calculated from only the CRP drying rates. It can also be seen from Figure 4 and Figure 6 that the differences between vacuum and steam drying CRP rates are greater than those between vacuum and steam drying calculated from combined CRP and FRP rates. This is due to the fact that in FRP the resistances to heat and mass transfer of superheated steam drying are lower than those of vacuum drying because the drying medium of steam drying was water. These effects of FRP drying rates therefore increase the values of the combined (or overall) drying rates of superheated steam drying and hence led to smaller differences between the overall drying rates of vacuum and steam drying.

In addition, it can be seen from Figure 6(a) that the inversion temperature calculated from combined CRP and FRP rates (109°C) is higher than the inversion temperature calculated from only CRP rates (93°C) of Figure 4(a). This is because towards the end of FRP of low-pressure superheated steam drying the drying rates are lower than those of vacuum drying since the equilibrium moisture content of particles in low-pressure superheated steam environment is higher and hence there is a lower driving force for moisture transfer. This is ascribed to the fact that the drying chamber has higher humidity values than the drying chamber in vacuum drying. As mentioned earlier, the equilibrium moisture contents of particles dried using LPSSD were higher than those dried using vacuum drying (see Figure 2). At higher operating pressures (say, 13 kPa) the equilibrium moisture contents of particles dried in a low-pressure superheated steam dryer are even higher and these lead to reduction of the combined rates of drying of the low-pressure superheated steam drying. Therefore, at higher operating pressures the intersection points of equal rates of drying might not even be accomplished (see Figures 6(b), 6(c)).

Mathematical modeling

Simple mathematical models that enable prediction of the drying curves of molecular sieves undergoing LPSSD and vacuum drying were developed based on the well-known Page's equation, ¹¹ single-term exponential equation and two-term exponential equation (Arrhenius-type model).

Page's equation

$$MR = \frac{X_t - X_{eq}}{X_i - X_{eq}} = exp(-kt^n)$$
 (1)

The parameters k and n in the equation were determined from the experimental data and were correlated as follows:

For LPSSD

$$k = -2.39 \times 10^{-1} + 2.86 \times 10^{-3} T - 7.13 \times 10^{-3} P - 3.83 \times 10^{-6} TP + 5.42 \times 10^{-2} \ln P$$

$$R^2 = 0.95$$

$$n = 1.87 - 3.91 \times 10^{-3} T + 1.11 \times 10^{-1} P - 5.44 \times 10^{-4} TP - 4.35 \times 10^{-1} \ln P$$

$$R^2 = 0.86$$

For vacuum drying

$$k = -7.42 \times 10^{-2} - 7.07 \times 10^{-5} T - 1.01 \times 10^{-2} P + 1.22 \times 10^{-5} TP + 1.12 \times 10^{-1} \ln P$$

$$R^2 = 0.96$$

$$n = 1.12 - 2.40 \times 10^{-3} T - 7.88 \times 10^{-2} P + 4.92 \times 10^{-4} TP + 2.21 \times 10^{-1} \ln P$$

$$R^2 = 0.73$$

Single-term exponential equation

$$MR = \frac{X_t - X_{eq}}{X_i - X_{eq}} = a \exp(-bt)$$
 (2)

For LPSSD

$$a = 1.12 - 1.41 \times 10^{-3} T + 4.53 \times 10^{-3} P - 6.87 \times 10^{-6} TP + 6.53 \times 10^{-3} ln P$$

$$R^2 = 0.75$$

$$b = -6.15 \times 10^{-2} + 1.12 \times 10^{-3} T - 9.75 \times 10^{-3} P + 7.56 \times 10^{-5} TP + 3.77 \times 10^{-2} \ln P$$

$$R^2 = 0.91$$

For vacuum drying

$$a = 9.68 \times 10^{-1} + 1.22 \times 10^{-3} T + 1.59 \times 10^{-4} P - 2.73 \times 10^{-5} TP - 1.12 \times 10^{-1} \ln P$$

$$R^2 = 0.94$$

$$b = 1.97 \times 10^{-2} - 3.74 \times 10^{-4} T - 2.13 \times 10^{-2} P + 1.08 \times 10^{-4} TP + 1.03 \times 10^{-1} ln P$$

$$R^2 = 0.70$$

Two-term exponential equation

$$MR = \frac{X_{t} - X_{eq}}{X_{i} - X_{eq}} = a_{1} \exp(-b_{1}t) + c_{1} \exp(-d_{1}t)$$
(3)

For LPSSD

$$a_1 = (0.699P^{-0.051})exp(-51.312/T_{abs})$$

$$R^2 = 0.62$$

$$b_1 = (354.576P^{-0.0267})exp(-2958/T_{abs})$$

$$R^2 = 0.95$$

$$c_1 = \left(5.63 \times 10^{-3} \, P^{0.408}\right) exp\left(-1269.76 / T_{abs}\right)$$

$$R^2 = 0.59$$

$$d_1 = (827.98P^{-0.132})exp(-3175.72/T_{abs})$$

$$R^2 = 0.93$$

For vacuum drying

$$a_1 = (3.709P^{0.554})exp(-1056.055/T_{abs})$$

$$R^2 = 0.53$$

$$b_1 = (0.164P^{0.059})exp(-185.677/T_{abs})$$

$$R^2 = 0.49$$

$$c_1 = \left(1.63 \times 10^{-3} \, P^{-1.082}\right) exp\left(2773.12/T_{abs}\right)$$

$$R^2 = 0.75$$

$$d_1 = (4.73 \times 10^{-2} P^{-0.903}) exp(871.105/T_{abs})$$

$$R^2 = 0.95$$

The equations were fitted with experimental data; the fitted equations were evaluated based on their R^2 and standard error of estimation. Comparing the three drying models, the results show that Page's equation fits the experimental data better than single-exponential equation and two-term exponential equation in the case of LPSSD, while single-exponential equation fits the experimental data well in the case of vacuum drying at operating temperatures in the range of 80° - 100° C and pressure of 7- 13 kPa as exemplified in Figures 7 and 8. The minimum R^2 of Page's equation was 0.997 and its maximum standard error of estimation was 0.0181 in the case of LPSSD while the minimum R^2 of single-term of exponential equation was 0.998 and its maximum standard error was 0.0233 in the case of vacuum drying. Drying constants of Page's equation (k and k) and of single-term exponential equation (k and k) are found to depend on the operating temperature as well as pressure.

Concluding remarks

Effects of operating parameters, i.e., drying temperature and pressure, on the rates of vacuum and low-pressure superheated steam drying of model porous particles were investigated experimentally in this study. In addition, the values of the inversion temperature calculated only from the rates of drying in the constant rate period were compared with those calculated from the whole drying period (constant rate period and falling rate period) in order to point out the fundamental differences between the two sets of temperatures beyond which the drying rates in low-pressure superheated steam drying were higher than those in vacuum drying. It was found that the inversion temperatures calculated from combined CRP and FRP rates was higher than the inversion temperatures calculated from only CRP rates. At higher operating pressures the intersection points of equal rates of drying might not even be obtainable. Empirical models which describe the experimental drying curves are also proposed. It is found that the Page's equation and single-term exponential equation can fit well the experimental data for LPSSD and

vacuum drying, respectively, over the ranges of operating temperature of 80-100°C and pressure of 7-10kPa.

Acknowledgements

The authors would like to express their sincere appreciation to the Thailand Research Fund (TRF), National Science and Technology Development Agency (NSTDA) and the International Foundation for Science (Sweden) for supporting this study financially.

Nomenclature

a = constant of single-term exponential model, -

 a_1 = constant of two-term exponential model, -

b = constant of single-term exponential model, -

 b_1 = constant of two-term exponential model, -

 c_1 = constant of two-term exponential model, -

 d_1 = constant of two-term exponential model, -

k = constant of Page's equation, -

MR = moisture ratio, -

n = constant of Page's equation, -

P = absolute pressure, kPa

t = drying time, min

 $T = \text{temperature of drying medium, } ^{\circ}\text{C}$

 T_{abs} = temperature of drying medium, K

 X_{eq} = equilibrium moisture content, kg/kg, (d.b.)

- X_i = initial moisture content, kg/kg, (d.b.)
- X_t = moisture content at any time, kg/kg, (d.b.)

Literature cited

- (1) Mujumdar, A. S. Superheated steam drying Technology of the future. pp. 115-138, In *Mujumdar's Practical Guide to Industrial Drying*; Devahastin, S., Ed.; Exergex: Brossard, Canada, 2000.
- (2) Kumar, P.; Mujumdar, A. S. Superheated-steam drying: A bibliography. *Drying Technol.* **1990**, *8*, 195.
- (3) Elustondo, D.; Elustondo, M. P.; Urbicain, M. J. Mathematical modeling of moisture evaporation from foodstuffs exposed to subatmospheric pressure superheated steam. *J. Food Eng.* **2001**, *49*, 15.
- (4) Shibata, H.; Mada, J.; Shinohara, H. Drying mechanism of sintered spheres of glass beads in superheated steam. *Ind. Eng. Chem. Res.* **1988**, *27*, 2353.
- (5) Shibata, H.; Mada, J.; Funatsu, K. Prediction of drying curves on sintered spheres of glass beads in superheated steam under vacuum. *Ind. Eng. Chem. Res.* **1990**, *29*, 614.
- (6) Senda, Y.; Bando, Y.; Yasuda, K.; Nakamura, M.; Sugimura, Y.; Shibata M. Development of superheated steam dryer at reduced pressure. In *Proc. the 1st Asia -Pacific Drying Conf.*, Bali, Indonesia, **2001**, 247.
- (7) Elustondo, D. M.; Mujumdar, A. S.; Urbicain, M. J. Optimum operating conditions in drying foodstuffs with superheated steam. *Drying Technol.* **2002**, *20*, 381.
- (8) Elustondo, D.; Elustondo, M. P.; Urbicain, M. J. Drying with superheated steam: Maximum drying rate as a linear function of pressure. *Chem. Eng. J.* **2002**, *86*, 69.
- (9) Devahastin, S.; Suvarnakuta, P.; Soponronnarit, S.; Mujumdar, A. S. A comparative study of low-pressure superheated steam and vacuum drying of a heat-sensitive material. *Drying Technol.* **2004**, in press.

- (10) Shibata, H.; Mada, J.; Shinohara, H.; Steam drying of sintered glass bead spheres under vacuum. *Ind. Eng. Chem. Res.* **1988**, *27*, 2385.
- (11) Page, G. Factors influencing the maximum rates of air drying shelled corn in thin layers. Master's Thesis, Purdue University, West Lafayette, Indiana, 1949.

Figure captions

- Figure 1. Schematic diagram of the low-pressure superheated steam dryer and associated units
- Figure 2. Drying curves of molecular sieve particles
- **Figure 3.** Drying rate curves of molecular sieve beads undergoing LPSSD and vacuum drying at various operating pressures
- **Figure 4.** Constant-rate period evaporation rates of moisture from molecular sieve beads at various operating pressures
- **Figure 5.** Effect of operating pressure on inversion temperature (based on CRP drying rates) of molecular sieve beads
- **Figure 6.** Average rate (CRP+FRP) of moisture removal from molecular sieve beads at various operating pressures
- Figure 7. Comparison of fitted models with the experimental data in the case of LPSSD
- Figure 8. Comparison of fitted models with the experimental data in the case of vacuum drying

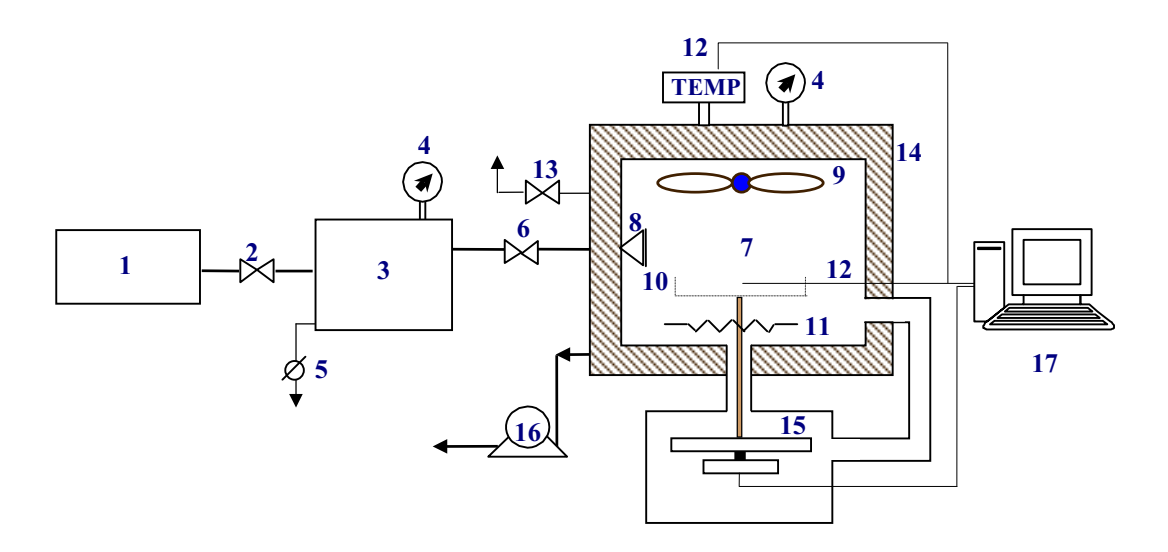


Figure 1. A schematic diagram of the low-pressure superheated steam dryer and associated units 1, boiler; 2, steam valve; 3, steam reservoir; 4, pressure gauge; 5, steam trap; 6, steam regulator; 7, drying chamber; 8, steam inlet and distributor; 9, electric fan; 10, sample holder; 11, electric heater; 12, on-line temperature sensor and logger; 13, vacuum break-up valve; 14, insulator; 15, on-line weight indicator and logger; 16, vacuum pump; 17, PC with installed data acquisition card

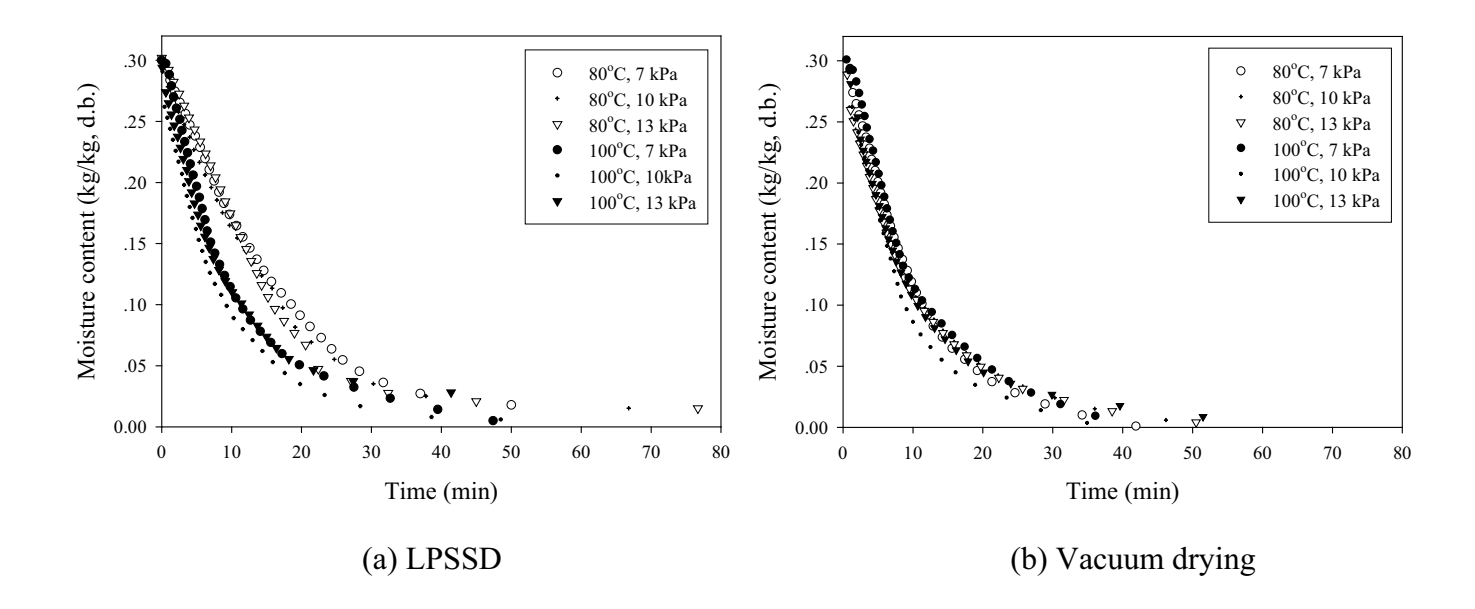


Figure 2. Drying curves of molecular sieve particles

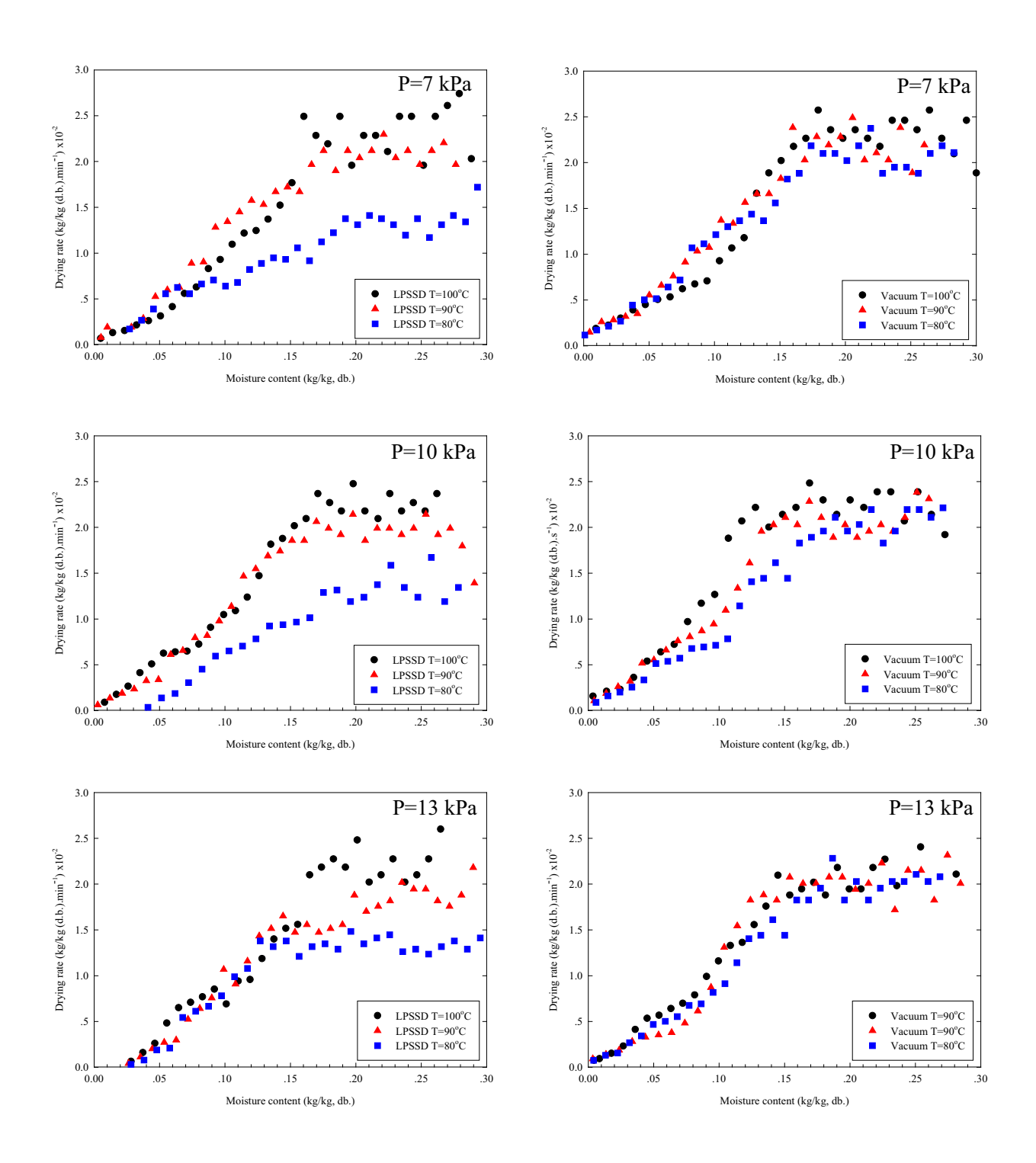


Figure 3. Drying rate curves of molecular sieve beads undergoing LPSSD and vacuum drying at various operating pressures

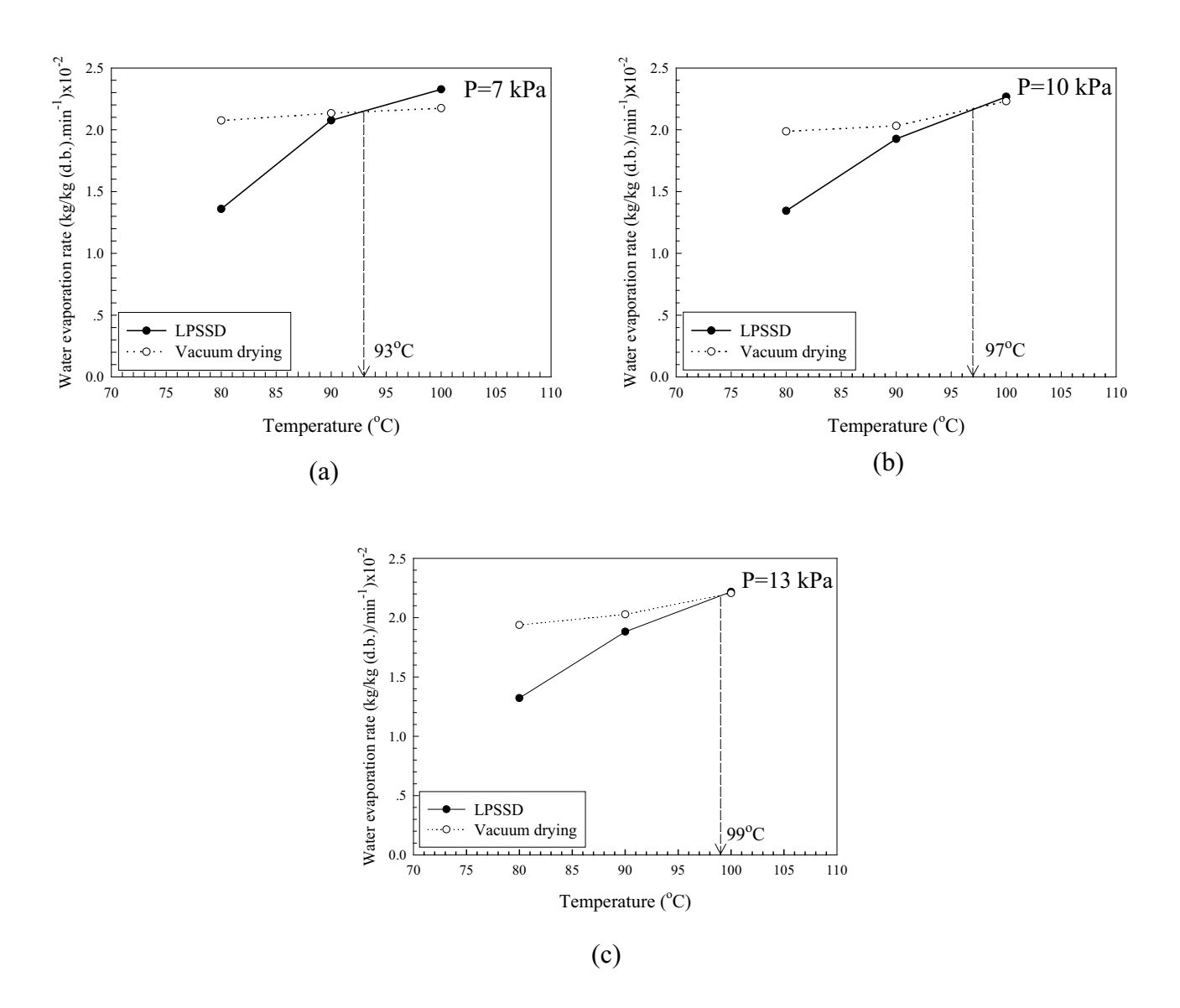


Figure 4. Constant-rate period evaporation rates of moisture from molecular sieve beads at various operating pressures

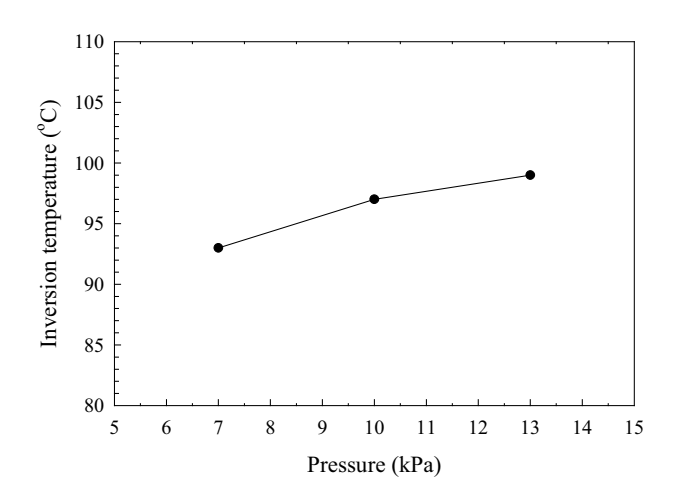


Figure 5. Effect of operating pressure on inversion temperature (based on CRP drying rates) of molecular sieve beads

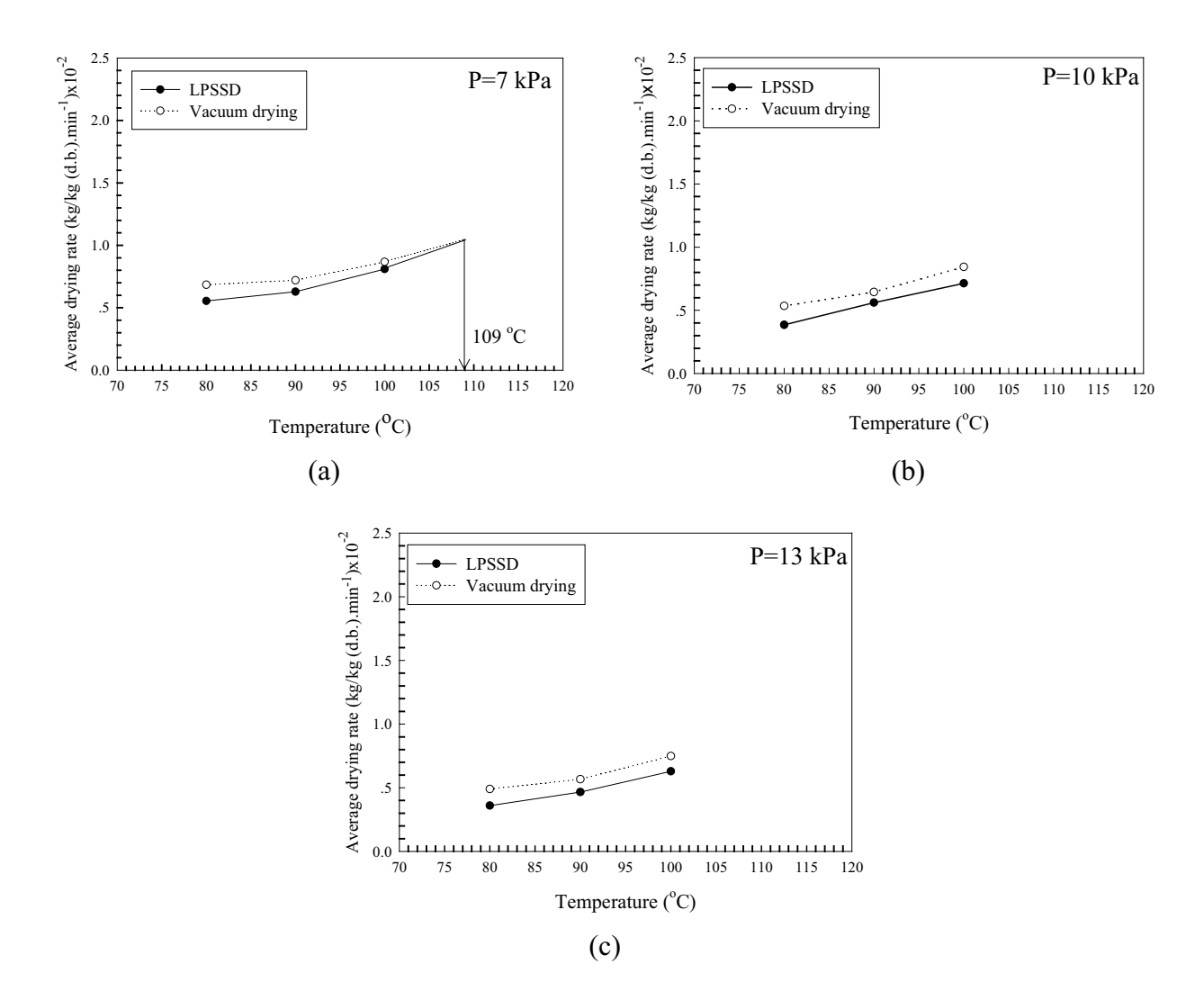
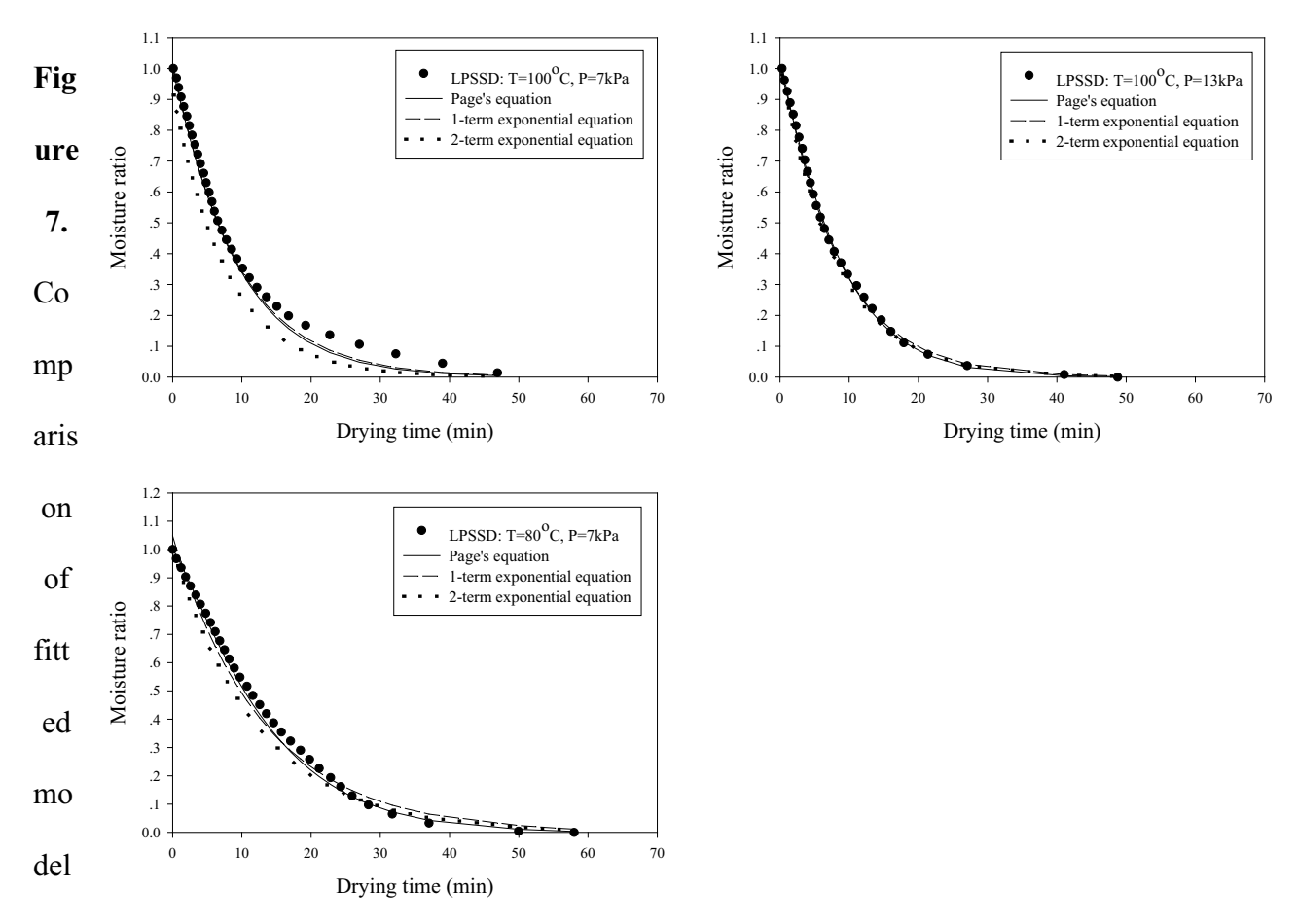
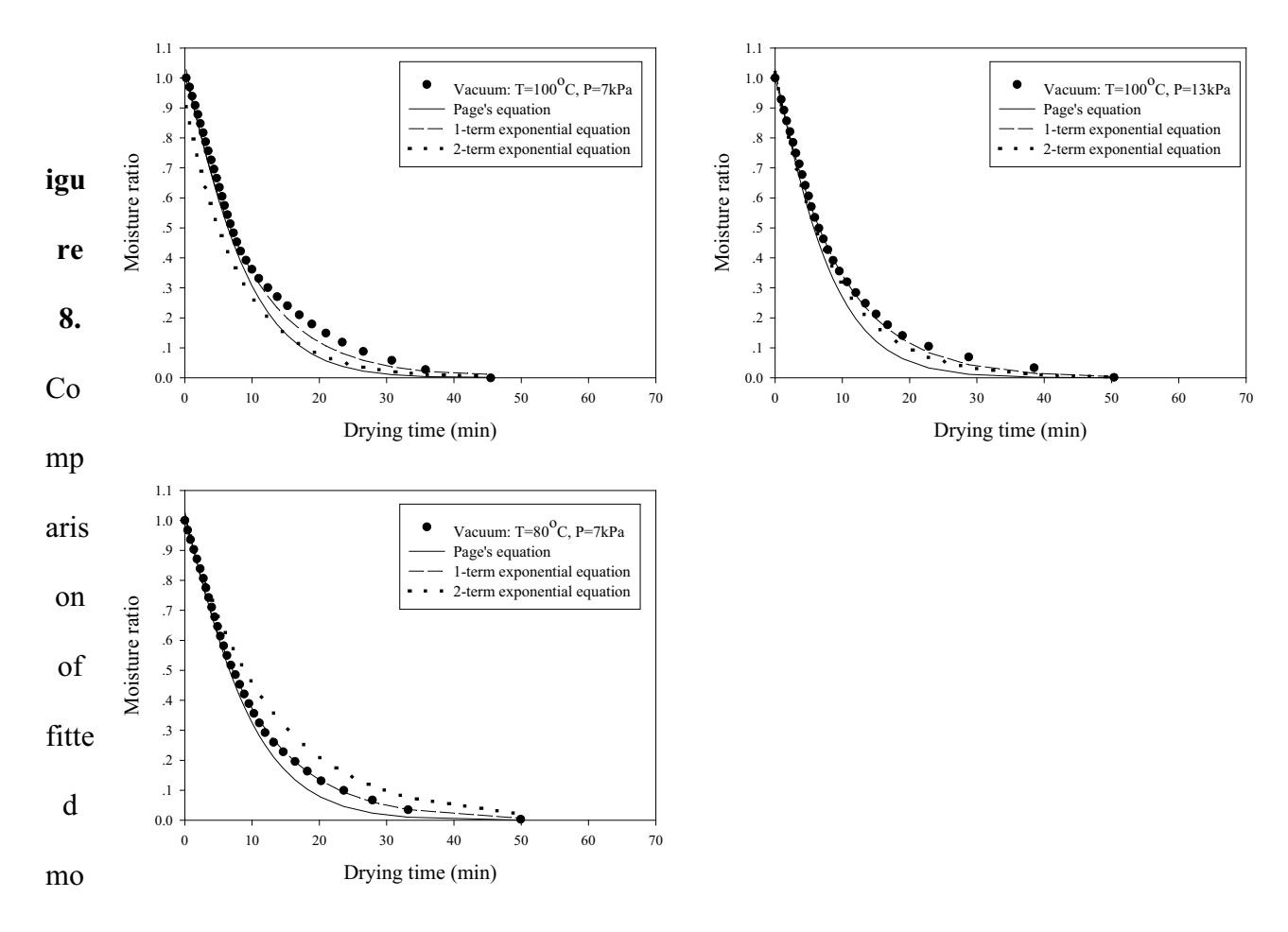


Figure 6. Average rate (CRP+FRP) of moisture removal from molecular sieve beads at various operating pressures



s with the experimental data in the case of LPSSD



dels with the experimental data in the case of vacuum drying